DEVELOPMENT OF MASS SPECTROMETRIC STRATEGIES

FOR LIPID CHARACTERIZATION AND MAPPING

A Thesis

by

LICHENG FAN

Submitted to the Office of Graduate and Professional Studies of
Texas A&M University
in partial fulfillment of the requirements for the degree of

MASTER OF SCIENCE

Chair of Committee,	Xin Yan
Committee Members,	David H. Russell
	Christian B. Hilty
	Yang Ni
Head of Department,	Simon W. North

August 2020

Major Subject: Chemistry

ABSTRACT

Lipids are primary components of cell membrane and play crucial roles in many biological functions such as energy storage and signal transduction. The aberrant metabolism of lipids is involved in the pathogenesis of many human diseases. The study of lipid structures and their spatial distributions in tissue samples is of great importance to describe lipid metabolism, discover disease biomarkers and understand disease mechanism.

Lipids display remarkable structural diversity, which is caused by many factors such as variable acyl chain lengths, unsaturation levels, substitutional positions and geometries. These factors allow the existence of various lipid isomers, which results in a significant challenge of accurate and rapid lipid structural identification. High resolution mass spectrometry (MS) coupled with tandem MS can readily differentiate chain length isomers and head group isomers. However, the structural differences between isomers can be very subtle, although they have dramatically different biochemical consequences, and cannot be directly identified through conventional MS.

To this end, the first project in the thesis describes the development of a mass spectrometric strategy that uses an alternating current to initiate i) electrospray (ES) for mass spectrometric analysis, and ii) electro-epoxidation of double bonds in unsaturated

lipids when positive voltage is applied to the electrode. The formed epoxides can generate diagnostic fragments in tandem MS to locate double bonds and can be detected in both positive and negative ion modes. The feasibility of this method has been illustrated using a lipid mixture with both positively-charged and negatively-charged lipids. The results show the successful identification of over 30 different lipid isomers in the lipid extracts of a mouse brain.

A sufficient characterization of lipids in a tissue sample requires not only structural identification but also their spatial distribution. The classic bulk “bind and grind” sample preparation for MS analysis homogenizes the lipids in tissue samples, and loses the spatial information of lipids in tissues. In the second project, desorption electrospray ionization-mass spectrometry imaging (DESI-MSI) was used to spatially map lipids in the mouse brain from an alcoholism model. Assisted by partial least squares-discriminant analysis (PLS-DA), a potential lipid biomarker at *m/z* 841.5 (tentatively identified as triacylglycerol 51:3) has been identified in dorsal striatum that shows lower intensity in the alcoholism mouse group compared with the normal one.

Lipids with low abundance or low ionization efficiency may play an important role in biological process, while the lack of sensitive and specific methods limits the studies of them. The third project in the thesis develops a derivatization method for the detection of 2-arachidonoylglycerol (2-AG) using phenylboronic acid in nano-electrospray ionization-

MS analysis. 2-AG is an important lipid in endocannabinoid system with low abundance and low ionization efficiency. The charge tag formed by reacting with phenylboronic acid can be added to *cis*-diol of 2-AG, which facilitates its mass analysis. Additionally, the specificity has been largely improved compared to protonation method, which is shown by the differentiation of 2-AG in tissue samples from its isomers in the background.

ACKNOWLEDGEMENTS

I would like to express my deepest gratitude to my supervisor, Prof. Xin Yan, for her continuous support throughout my master research. Thank you for all your help with my experiments and your support for the decisions I made.

I would also like to thank Dr. Heyong Cheng, Shuli Tang, Dacheng Kuai and all other students from the Yan research group for giving me the opportunity to work in such a friendly and helpful laboratory environment.

I would like to thank my committee members, Prof. David H. Russell, Prof. Christian B. Hilty and Prof. Yang Ni, for their guidance and support throughout my research.

I would like to thank the Department of Chemistry at Texas A&M University and all the professional, technical and academic staff. Many thanks to the Head of Department, Prof. Simon W. North for all the support that I received.

Finally, I would like to thank my parents, for their support for any decisions I made and my friends, Leon Liu, Zachary Geng and Lingjue Wang for all the encouragement, patience and support during the past two years.

CONTRIBUTORS AND FUNDING SOURCES

Contributors

This work was supported by a thesis committee consisting of Professor Xin Yan, Professor David H. Russell, Professor Christian B. Hilty of the Department of Chemistry and Professor Yang Ni of the Department of Statistics.

The mouse brain slices for Section 3 was provided by Professor Jun Wang (Institute for Neuroscience, TAMU). The optical images of the nano-electrospray emitters in Section 2 and Section 4 were captured with the help from Dr. Heyong Cheng.

All other work conducted for the thesis was completed by the student independently.

Funding Sources

Graduate study was supported by Dr. Xin Yan's research startup funds from Texas A&M University.

NOMENCLATURE

MS	Mass spectrometry
NMR	Nuclear magnetic resonance
MS/MS	Tandem mass spectrometry
GC	Gas Chromatography
HPLC	High-performance liquid chromatography
PB	Paternò–Büchi
m-CPBA	*meta*-Chloroperoxybenzoic acid
SILD	Stable isotope-labeling derivatization
MSI	Mass spectrometry imaging
m/z	Mass-to-charge ratio
ESI	Electrospray ionization
SIMS	Secondary ion mass spectrometry
DESI	Desorption electrospray ionization
MALDI	Matrix-assisted laser desorption ionization
nanoESI	nano-Electrospray ionization
RF	Radio frequency
C-trap	Curved linear trap

HCD	High energy collisional dissociation
TLC	Thin layer chromatography
EC-MS	Electrochemistry coupled with mass spectrometry
WIE	Wire-in-emitter
CID	Collision-induced dissociation
PC	Phosphocholine
AC	Alternating current
DC	Direct current
FA	Fatty acid
LOD	Limit of detection
OCT	Optimal cutting temperature
AGC	Automatic gain control
TIC	Total ion chromatogram
ROI	Region-of-interest
PLS-DA	Partial least squares – discriminant analysis
SAM	Significance analysis of microarrays
VIP	Variable importance in projection
2-AG	2-Arachidonoylglycerol
1-AG	1-Arachidonoylglycerol

LC-MS/MS	Liquid chromatography-tandem mass spectrometry
PE	Phosphatidylethanolamine
Fmoc	Fluorenylmethoxylcarbonyl
FAME	Fatty acid methyl ester

TABLE OF CONTENTS

LIST OF FIGURES

LIST OF TABLES

LIST OF SCHEMES

1. INTRODUCTION

1.1 Overview of Lipids

Lipids are a diverse and ubiquitous group of biomolecules which play crucial roles in cellular physiology and pathology. Previous work has demonstrated that aberrant metabolism of lipids is involved in the pathogenesis of many human diseases such as obesity,[1] diabetes,[2] cardiovascular disease,[3] cancer,[4] neurodegenerative disorders,[5] and autoimmune diseases.[6,7] The capability to fully characterize lipid species is required to identify the lipid network for metabolic and gene regulation,[8-10] to discovery disease biomarkers,[11,12] and to understand disease mechanism.[13,14]

1.1.1 Lipid Structures and Biological Functions

Lipids are small hydrophobic or amphiphilic molecules that originate either entirely or partially from two distinct types of building blocks, namely ketoacyl and isoprene groups. However, different from the cases of DNA and proteins that are primarily composed of the linear combinations of 4 nucleic acids and around 20 amino acids, respectively, lipids are a diverse group of compounds with 8 main categories and over 200,000 estimated species.[15] The major lipid categories found in human plasma[16] are listed in **Scheme 1.1**.

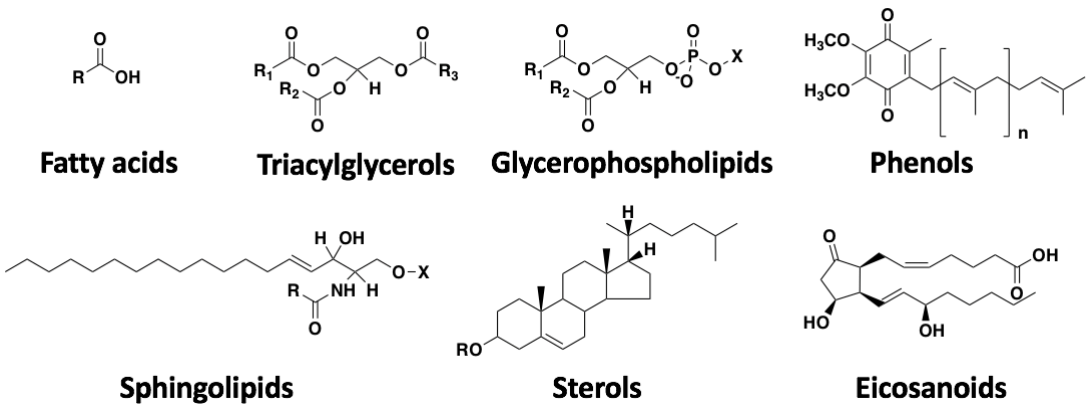

Scheme 1.1. Major lipid categories found in human plasma.

Associated with their hydrophobic or amphiphilic structures, lipids are essential cellular constituents that have multiple critical roles in cellular functions: i) Lipids help to form the vital membrane bilayers and provide a hydrophobic environment for protein functions; ii) lipids can also work as reservoirs for energy storage; iii) some membrane lipids are important messengers for signaling and intercellular regulations.[17-19] The major functions of lipids are illustrated in **Figure 1.1**.

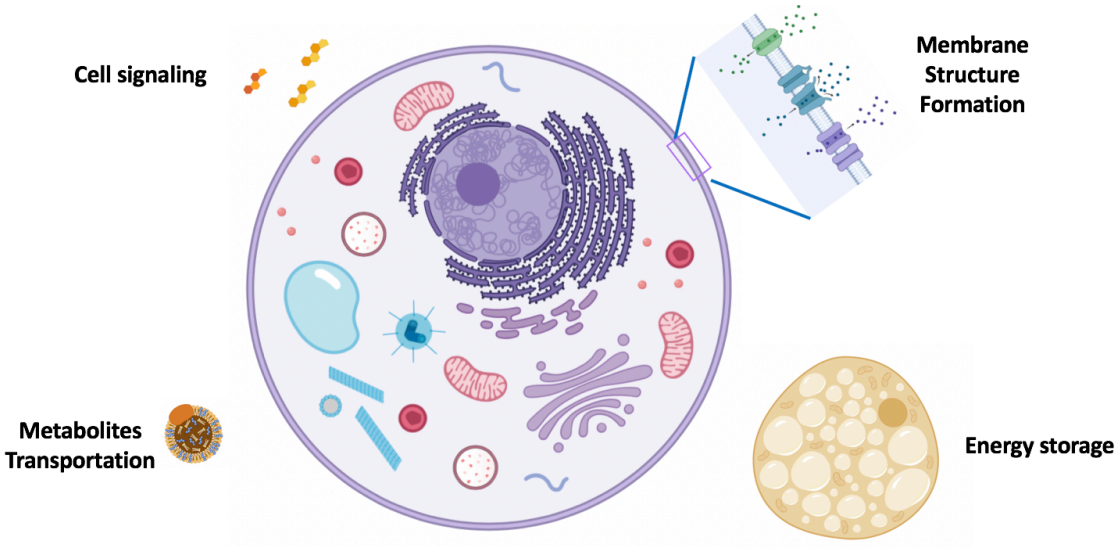

Figure 1.1. Schematic of major functions of lipids in the cell.

1.1.2 Isomers of Phospholipids

Phospholipids are a type of lipid molecules that are the main components of cell membranes. A phospholipid molecule consists of a hydrophilic head including a phosphate group, and hydrophobic fatty acid tails (**Figure 1.2**). Phospholipids can form lipid bilayers because of their amphiphilic features.[20] Additionally, phospholipids have been widely used to prepare liposome of drugs to improve bio-availability, reduce toxicity, and increase permeability.[21,22]

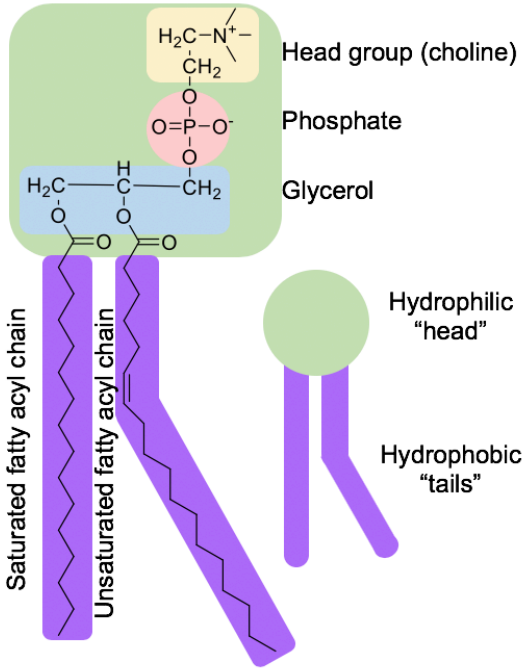

Figure 1.2. A typical structure of phospholipids.

A big challenge in the structural characterization of phospholipids is derived from their isomerism phenomenon. The diversity in chemical structures of phospholipids comes from the category of hydrophilic head groups, the different lengths of hydrophobic chains, the number and the location of double bonds, the binding positions of fatty acyl chains and the regiospecificity of aliphatic moieties.[23] Examples of phospholipid isomeric forms are listed in **Scheme 1.2**.

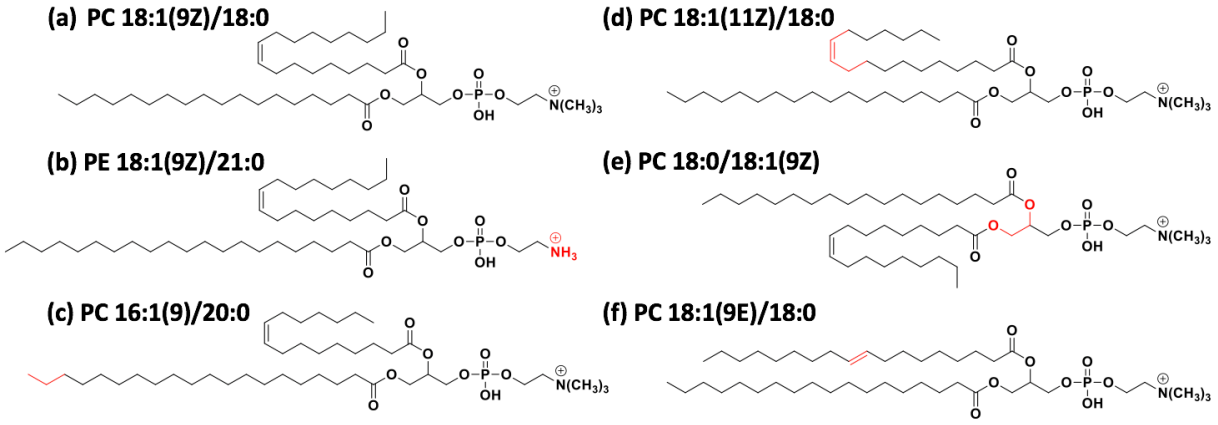

Scheme 1.2. Examples of possible isomeric forms of (a) phosphatidylcholine 18:1(9Z)/18:0 (*m/z* 788.6164) arising from (b) head group isomerism, (c) chain length isomerism, (d) double-bond positional isomerism, (e) *sn*-positional isomerism and (f) *cis/trans* isomerism.

The accurate identification of phospholipid structures is essential not only for mapping metabolic pathways and studying lipid-protein interactions,[24,25] but also for the pathological study of certain diseases.[26,27] For example, the alteration in chain length or degree of unsaturation is associated with the change in fluidity and functions of cellular membranes,[28-30] and the increased ratio of *trans*-fatty acyl chains is related to the increased risk of cardiovascular diseases and strokes.[31]

Currently, many modern technologies including mass spectrometry (MS), nuclear magnetic resonance (NMR) spectroscopy,[32] Raman spectroscopy,[33] and column chromatography[34] have been used in phospholipid isomer identification. Among them, MS has become an indispensable analytical technique because of its high sensitivity and

selectivity along with structural characterization capability. The exact molecular formulas measured from high-resolution MS and the fragmentation patterns obtained from tandem MS (MS/MS) through collision-induced dissociation (CID) can readily identify head group isomers and chain length isomers. However, other phospholipid isomers, such as *sn*-positional isomers, double-bond positional isomers, double-bond stereochemical isomers and enantiomers, can only be identified using novel derivatization strategies or with an external apparatus.

The localization of double bonds in unsaturated lipids is not only essential for a better understanding of *de novo* synthesized lipids from enzymatic processes,[35] but also relates to many disease progressions.[36,37] Thus, the accurate and rapid characterization of double-bond positional isomers has attracted more and more attention. Reported methods for double-bond localization in phospholipids include i) hyphenated techniques, such as gas chromatography (GC) or high-performance liquid chromatography (HPLC) coupled with MS;[38-40] ii) novel gas-phase fragmentation methods, such as high-energy collision-induced dissociation,[41] charge remote fragmentation,[42] and ultraviolet photodissociation;[43] iii) selective double-bond derivatization methods including ozonolysis,[40,44] and Paternò–Büchi (PB) reaction,[45] as well as plasma-induced,[46] offline *meta*-chloroperoxybenzoic acid (*m*-CPBA)[47] and electrochemical epoxidation.[48]

1.1.3 Detection of Low-abundance Lipids

MS is widely used in lipidomics owing to its capability of performing untargeted analysis, high-throughput studies, and compatibility with external apparatus. However, direct detection of low-abundance lipids in a complex sample using MS is limited by the ion suppression from high-abundance, and highly ionizable compounds.[49]

Even though some lipid species have relatively low abundances in tissue, they can play significant roles in metabolic pathway signaling and regulation. For example, a low-abundant signaling lipid, 3,5-bisphosphate phosphatidylinositol, is related to neurodegenerative diseases.[50] However, these lipids are not well detected and seen during an untargeted MS analysis.

In order to facilitate the detection of lipid species at trace level, hyphenated techniques including gas chromatography and high-performance liquid chromatography are usually coupled with mass spectrometry for pre-analysis separation.[51,52] Besides, these hyphenated techniques also have the ability to separate isomers and reduce ion-suppression effect. However, these techniques have some inherent difficulties including different ionization efficiency at different elution times, differential loss of lipids on the column, and non-uniform distributions of lipid species in eluted peaks.[53] All these difficulties limit their applications in the detection of low-abundance lipids.

An alternative method for low-abundance lipid detection is chemical derivatization.

Appropriate derivatization can improve analytical performance for targeted lipids with higher detection sensitivity and selectivity than the underivatized case. For example, the application of stable isotope-labeling derivatization (SILD) were used for the detection of neurosteroids in rat blood microdialysates with higher sensitivity and less matrix and ion suppression effects.[54]

1.1.4 Spatial Distributions of Lipids in Biological Tissues by Mass Spectrometry Imaging

For lipid analysis, a sufficient characterization requires not only the catalog of the lipids within the sample but also the spatial distributions of lipid species. The aberrant accumulations and migrations of certain lipid species are related to the pathogenesis of many human diseases.[55,56]

Mass spectrometry imaging (MSI) is a powerful tool that enables untargeted investigations into the spatial distributions of hundreds of lipid species in a single experiment without labeling. The combination of structural information obtained from mass spectrometry and visualization of lipid distributions in space makes MSI a valuable technique for biological sample characterization, disease mechanism discovery, and drug delivery study. For example, previously unknown cholesterol-rich ribbon-shaped areas in cerebellar white matter were identified through MSI research,[57] and different human astrocytoma subtypes can be differentiated and localized through MSI.[58]

1.2 Mass Spectrometry Based-Lipid Analysis

Mass spectrometry is a powerful analytical technique capable of providing qualitative and quantitative analysis. In mass spectrometric analysis, analytes are ionized by an ion source to form gas-phase ions, which are then detected by a mass analyzer based on their mass-to-charge ratios (*m/z* values).

Because of the diversity of lipids, lipid analysis is a challenge in the analytical community. Given its label-free detection, high sensitivity and structural characterization capability, mass spectrometry has become one of the most popular analytical techniques for lipid analysis. Through mass spectrometry, researchers can obtain accurate structural information of lipid species and map the distribution of lipid species through mass spectrometry imaging while maintaining high tolerance towards high salt concentration or complex solvent system. Major components of mass spectrometry are introduced in the following sections.

1.2.1 Ion Source of MS

Ion source is one of the key components in a mass spectrometer where analytes are converted into gas-phase ions. The choice of the ionization method can significantly impact mass spectrometric analysis in ionization efficiency, operation environment and online fragmentation patterns. Various ionization techniques have been used in mass spectrometry for lipid analysis including electrospray ionization (ESI), secondary ion mass

spectrometry, desorption electrospray ionization and matrix-assisted laser desorption ionization.

1.2.1.1 Electrospray Ionization

Electrospray ionization is one of the most widely used ionization methods in lipid analysis.[59] ESI is a soft ionization method that minimizes the degree of fragmentation during ionization. This method can ionize samples dissolved in polar solvents under atmospheric pressure and can readily interface with other analytical techniques such as liquid chromatography, which could further improve its performance.

In ESI, analytes are dissolved in polar solvents and then introduced into a capillary with a high voltage applied between the capillary and the MS inlet. The voltage induces the formation of charged droplets that spray out from the capillary tip. The presence of sheath gas (usually nitrogen gas) assists the directing of charged droplets spray into the MS inlet as well as the primary evaporation of the solvents. Afterward, the charged droplets pass through a heated capillary inside the MS inlet for complete solvent evaporation and the gas-phase ions are generated. **Figure 1.3** shows the electrospray ionization process.

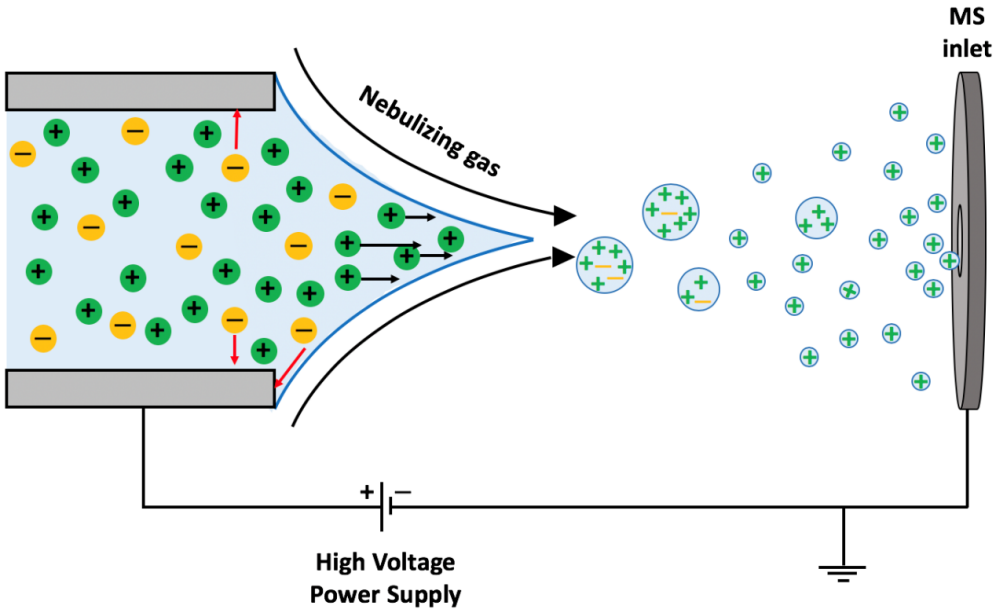

Figure 1.3. Schematic of electrospray ionization process.

1.2.1.2 nano-Electrospray Ionization

The sample amount for lipid analysis, especially in biological samples, is usually low. The development of nano-electrospray ionization (nanoESI) further extends the application of ESI technique in lipid analysis.[60] One major advantage of nanoESI is its low flow rate, which reduces the required amount of sample for analysis. While conventional ESI operates at a solution flow rate of 1~200 μL/min, nanoESI can produce a stable spray at a flow rate as low as 10 nL/min, and requires no sheath gas for desolvation.[61] Moreover, nanoESI has higher salt tolerance and lower matrix effects than conventional ESI. With all these advantages, nanoESI is often the technique of choice for lipid analysis.

1.2.2 Mass Analyzer

1.2.2.1 Linear Ion Trap

A linear ion trap confines ion radially by a two-dimensional radio frequency (RF) field together with stopping potentials applied to end electrodes. Afterwards, ions trapped in the linear tubes can either undergo collision-induced dissociation by buffer gas or get isolated through dipole or quadrupole excitation, which can be detected by a dual conversion dynode detector.

1.2.2.2 Orbitrap

The heart of the Orbitrap analyzer is an axially-symmetrical mass analyzer including a spindle-shaped central electrode surrounded by a pair of bell-shaped outer electrodes. Here, ions with an identical *m/z* value experience a same axial oscillation frequency but different radical and rotational motion frequencies. Thus, the ion pocket of a specific *m/z* ratio forms a thin ring and signals can be detected through differential amplification when this ring moving between different half outer electrodes.

Another two key components of the Orbitrap analyzer are curved linear trap (C-trap) and high energy collisional dissociation (HCD) collision cell. Ions lose their kinetic energy in collision with the nitrogen bath and get trapped near the middle part of the C-trap. A C-trap can store ions and minimize the pulse problem for Orbitrap. In HCD collision cell, collision gas is supplied for fragmentation and a potential gradient is used for the fast

extraction of ions. The overall layout of the Orbitrap mass analyzer is shown in **Figure 1.4**.

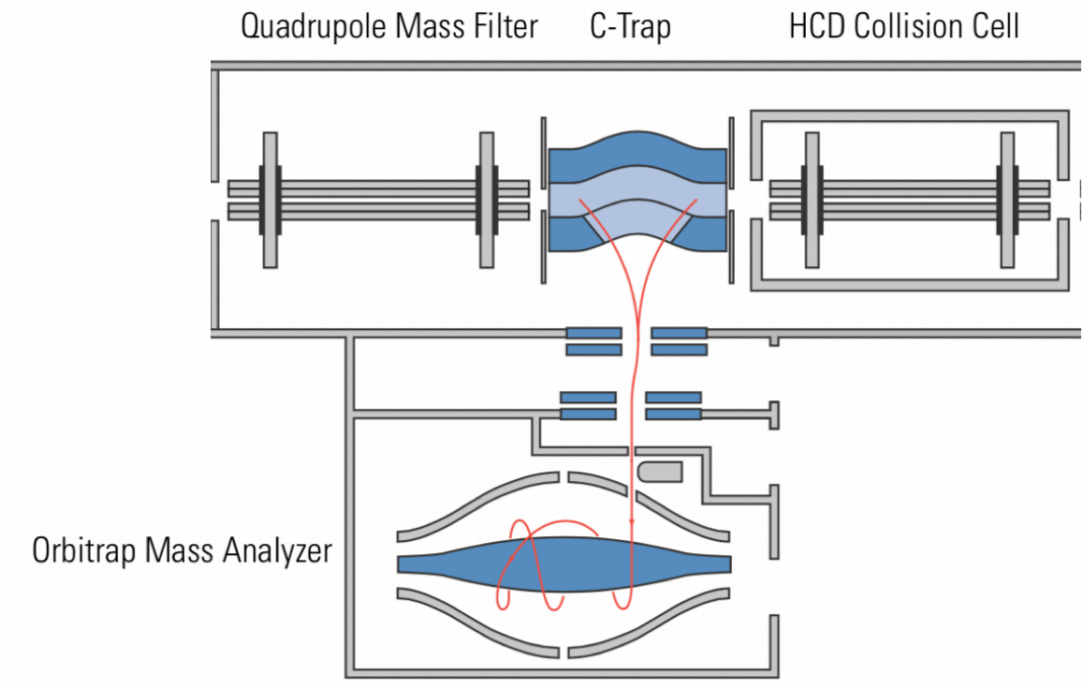

Figure 1.4. The configuration of an Orbitrap mass analyzer. (cited from "Orbitrap Velos Pro-Hardware Manual", Thermo Fisher Scientific Inc.)

1.3 Lipid Mass Spectrometry Imaging

The workflow for mass spectrometry imaging is summarized as below. Typically, after the collection of samples from the animal, researchers will embed the tissue samples in a supporting medium for the sectioning into slides. Some sample processing, such as the

application of matrix or derivatization agent, can be performed depending on the ionization methods and species of interest. Then, mass spectra are collected at all grids with manually defined pixel size across the section. All collected spectra are used to computationally reconstruct the heat map image depicting the distribution of a certain *m/z* value. Finally, statistical workflows and machine learning algorithms are implemented to handle the large imaging data sets and provide significant information for further physiological and pathological study.

Among all the steps described above, the ionization methodology is one of the most important processes in MSI, which determines the sensitivity, selectivity, and spatial resolution of the research. Three most commonly used MSI ion sources for lipid analysis are secondary ion mass spectrometry, matrix-assisted laser desorption /ionization and desorption electrospray ionization.[62]

1.3.1 SIMS and MALDI

Secondary ion mass spectrometry (SIMS) uses high-energy primary ions to strike the sample surface and the induced collision cascade releases the secondary ions from the surface, which are detectable using sequential mass analyzers. In practical applications, SIMS is usually the method of choice for subcellular pharmaceutical investigations because it can reliably achieve spatial resolution down to the nanometer range.[63] However, SIMS is often limited to analyzing molecules under 1000 Daltons due

to the extensive surface fragmentation.[64]

In contrast to SIMS that requires no sample preparation, matrix-assisted laser desorption ionization (MALDI)-MSI requires the tissue to be coated with a thin layer of matrix. The matrix absorbs the energy from the incident laser beam and provides ionization for analyte compounds in a “soft” manner. MALDI-MSI has the advantages of broad applicability and high sensitivity at an excellent lateral resolution.[64,65]

1.3.2 DESI-MSI

Different from the two ionization techniques mentioned above, desorption electrospray ionization (DESI) is an ambient ionization method, which means the ionization occurs at atmospheric pressure with the samples being analyzed in their native state. There are several advantages using ambient ionization: i) there is no or minimal sample preparation prior to the sample analysis, which helps to maintain the morphology and original distribution of lipids; ii) ambient MSI avoids the trouble with vacuum situation and is easier to implement; iii) ionization by spray-based ambient ionization methods is soft. The low average internal ionization energy deposition can minimize fragmentation during ionization.

Reported firstly in 2006 by Dr. Cooks group, DESI-MSI has a broad range of applications.[66] First, DESI-MSI has the capability for lipid profiling, providing the spatial distributions of particular lipids with structural information.[67] Besides, DESI-MSI can be

coupled with crude separation steps, such as thin layer chromatography (TLC), for organic reaction monitoring and complex biological samples analysis.[68,69] Finally, DESI-MSI of biological tissues were also used for tissue characterization and disease state evaluation. For example, the diagnostics and region discrimination of many types of cancerous tissues were conducted using DESI-MSI.[70]

In performing DESI-MSI, a spray of charged micro-droplets from a pneumatically-assisted electrospray needle is directed to the targeted pixel on the sample surface and undertakes desorption of the analytes into the gas-phase and subsequent ionization through collision. The ionization process of DESI is illustrated in **Figure 1.5**.

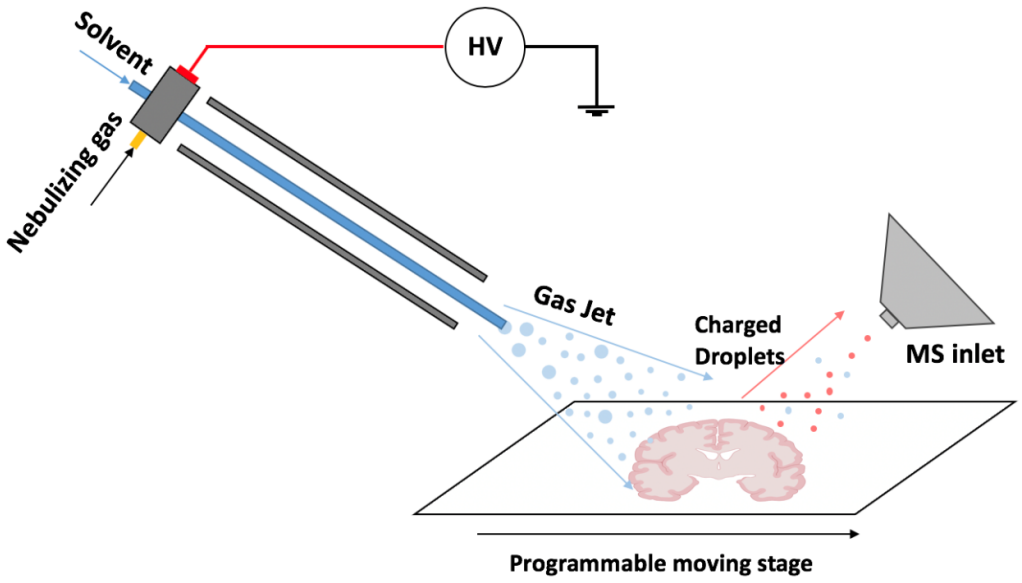

Figure 1.5. Illustration of desorption electrospray ionization process.

2.DEVELOPMENT OF AN ELECTROCHEMICAL MASS SPECTROMETRIC METHOD FOR DOUBLE-BOND LOCALIZATION IN UNSATURATED LIPIDS

2.1 Introduction

Lipids are fundamental building blocks of cells and play many important roles in cellular physiology and pathology. The existence of lipid isomers makes the lipid structural characterization challenging. In recent years, the characterization of lipid double-bond positional isomers has been the focus of extensive research and significant progress has been made. Highlights of this topic include gas-phase fragmentation methods and selective double-bond derivatization methods such as online electrochemical epoxidation.

Electrochemistry coupled with mass spectrometry (EC-MS) is a powerful tool for identifying the products and intermediates of electrochemical reactions. In particular, the electrochemical nature of the electrospray ionization allows the wide application of electrochemistry for chemical analysis.[71] In ESI, the current is generated upon the application of a high voltage between the spray capillary and the MS inlet. Therefore, an ESI source is analogous to a floated emitter system and can be used to induce electrochemical reactions.

Recently, our group has reported a novel strategy that combines an on-demand electrochemical epoxidation with nano-electrospray ionization/tandem mass

spectrometry (nanoESI-MS/MS) for double-bond localization in unsaturated phospholipids.[48] This method has many advantages including voltage-dependent derivatization of lipids, low sample consumption and no requirements for extra apparatus. However, electro-epoxidation of lipids only occurs when positive voltage is applied to the nanoESI electrode (anode), which limits the direct detection of negatively charged lipids. For negatively charged lipids, lithium ions are added to the solution which convert lipids to the positively charged formats followed by electro-epoxidation to locate the double bonds. The addition of lithium ions can cause ion suppression of native positively charged lipids, which cannot be well detected in the same system simultaneously.

In this section, an electrochemical mass spectrometric strategy for direct detection of unsaturated lipids in both positive and negative ion modes is developed. An alternating current (AC) electric field is used for initiating electro-epoxidation of all unsaturated lipids in the positive half work cycle while generating electrospray at both positive and negative ion modes, respectively. The feasibility of negatively charged lipid detection and simultaneous detection in both ion modes has been demonstrated. The lipid extracts of mouse brain were also analyzed and a lipid catalog with identification of double-bond positional isomers was obtained.

2.2 Materials and Methods

2.2.1 Mass Spectrometry

2.2.1.1 Ion Source

NanoESI source with a big-orifice (60 μm) emitter was used in this experiment. Single-channel borosilicate capillary tubes (0.86 mm I.D. and 1.5 mm O.D., #1B160-6, World Precision Instruments, Sarasota, FL) were used for the big-orifice nanoESI emitter fabrication. Borosilicate capillary tubes were pulled using a P-1000 Flaming/Brown micropipette puller (Sutter Instrument Company Co., Novato, CA).

The following parameters were used for the big-orifice nanoESI emitter fabrication: the HEAT value was set to be 525 with a ramp value of 490. PULL value was set at 0 and the VELOCITY value was 3 with TIME at 250 and PRESSURE at 500. Emitter tip geometries were characterized using an optical microscope. Characterization of the emitter tips was performed through the measurement of the emitter orifice size and the shape of the orifice. The image of a big-orifice nanoESI emitter is shown in **Figure 2.1**. The average size for the big-orifice nanoESI emitters is ~ 60 μm.

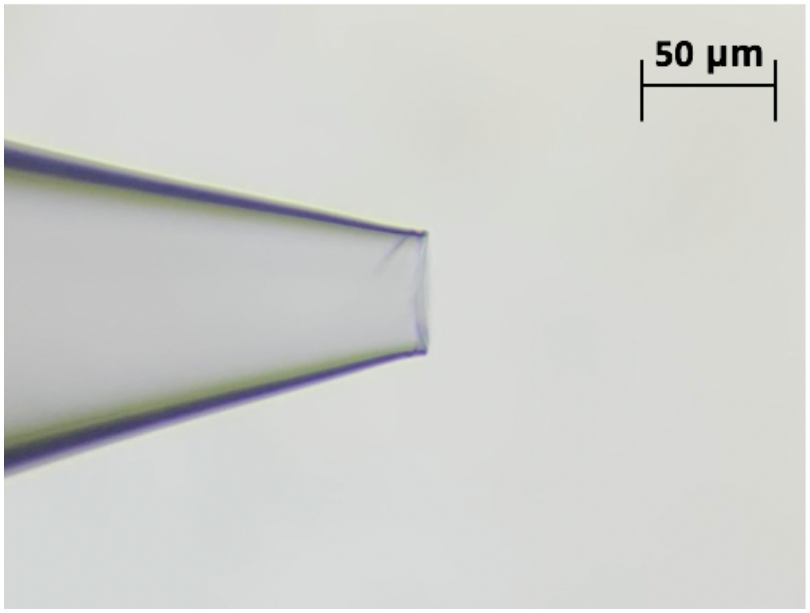

Figure 2.1. The optical image of a big-orifice nanoESI emitter.

2.2.1.2 Power Supply

A high potential difference between the nanoESI electrode and a counter electrode is required in nanoESI to maintain the electrospray. Wire-in-emitter (WIE) technique was used in the research for high voltage supply. A platinum wire (400 µm in diameter) was inserted inside the nanoESI emitter and connected to the high voltage AC power supply. The configuration of the nanoESI ion source is shown in **Scheme 2.1**.

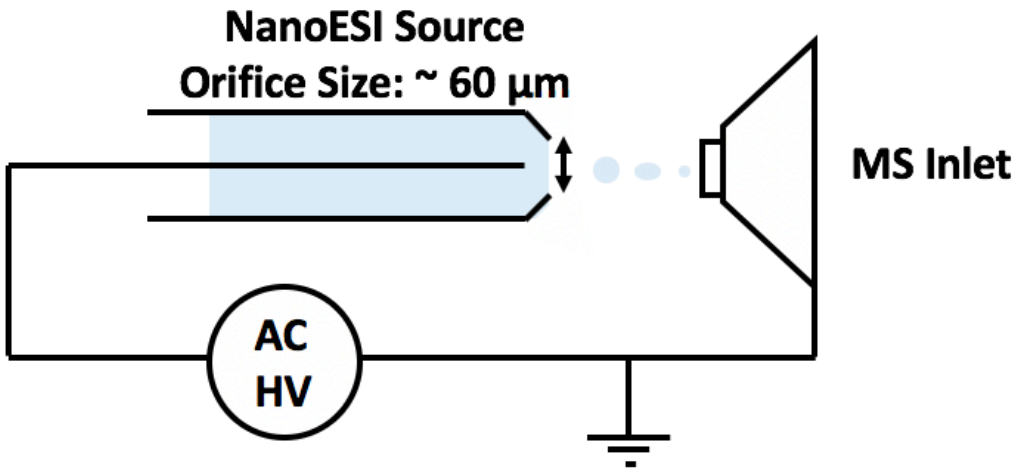

Scheme 2.1. The configuration of alternating current induced nano-electrospray ionization source.

The AC voltage was induced by a high-voltage AC power supply (**Figure 2.2**). The AC voltage (0 ~ ±4 V) was originally generated from a synthesized function generator (Model DS345, 30 MHz, Stanford Research Systems, Sunnyvale, CA), followed by a high-voltage amplifier (Model 609D-6, 0 ~ ±4kV, Trek, Lockport, NY) for a 1000-fold amplification. The output voltage was monitored with a digital storage oscilloscope (DSO5102P, 100MHz, 1GSa/s, Hantek Electronic Co., Ltd, Qingdao, China).

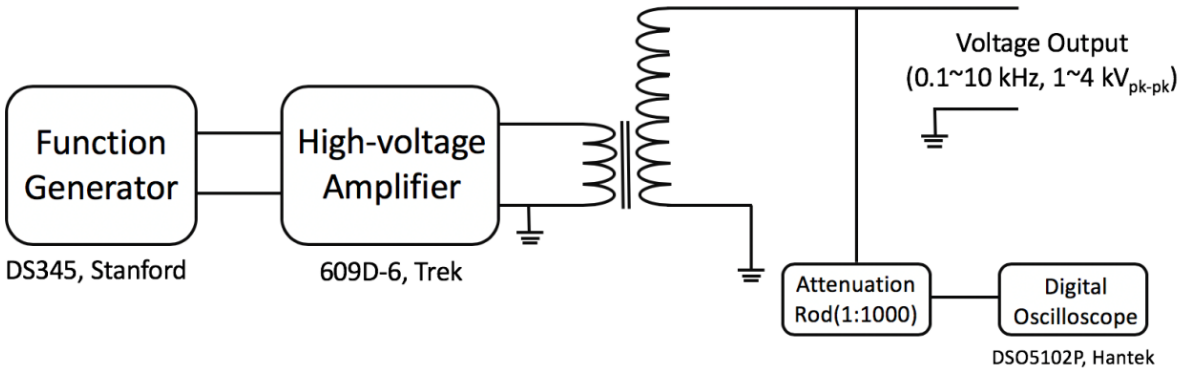

Figure 2.2. The configuration of the high-voltage AC power supply.

2.2.1.3 Mass Analyzer

LTQ-Velos Pro-Orbitrap (Thermo Fisher Scientific Inc.) was the mass analyzer used in this study. The following parameters were used for data acquisition: capillary temperature 275 °C, S-lens RF level 67.6% in positive ion mode, and capillary temperature 275 °C, S-lens RF level 60% in negative ion mode, maximum injection time 500 ms and 1 microscan for each individual scan, mass resolution at 60,000. Full mass spectrum scans were acquired at *m/z* 100-500 in negative ion mode and 200-1000 in positive ion mode. Tandem mass spectra were obtained via collision-induced dissociation with a normalized collision energy of 30.

2.2.2 Lipid Extraction Procedure

Folch method was used for lipid extraction in this study.[72] The frozen brain sample

was dried in a vacuum desiccator for 15 min. A small amount (26.1 mg) of brain sample was sectioned from the whole mouse brain and transferred to 400 μL of chloroform: methanol (2:1, v/v) solvent. The mixture was homogenized using a mini homogenizer for 6 minutes until there were no clear chunks of tissues. The homogenate was then centrifuged at 4500 rpm for 5 min. The supernatant was separated and filtered with a syringe filter with 0.22 μm pore size. The extraction was repeated for three times. The supernatants were combined and mixed thoroughly with 400 μL of water. The mixture was centrifuged at 4500 rpm for 5 minutes. The top MeOH/water layer was removed from the system. The water-wash step was repeated twice. Finally, 450 μL of methanol was added to dissolve the fluffy white layer and 800 μL of lipid extraction was generated for further analysis.

2.3 Results

2.3.1 AC-Induced Electro-Epoxidation of Lipid Double Bonds

The feasibility of AC-ESI combined with electro-epoxidation of lipids was shown using PC 18:1(Δ6)-18:1(Δ6), an unsaturated phosphocholines (PC). PC 18:1(Δ6)-18:1(Δ6) (20 μM) was dissolved in acetonitrile/water (80/20, v/v) containing 10 mM HCl and loaded in a big-orifice nanoESI emitter. Upon the application of 6 kV AC voltage ($V_{pk\text{-}pk}$, 100 Hz, square wave, same as below), a stable electrospray was generated and only the protonated PC peak at *m/z* 786.67 was observed (**Figure 2.3a**). When a lower AC

voltage at 4 kV was applied to the electrode, a meniscus with a large surface was formed, where a droplet flow was sprayed out of the meniscus. Meanwhile, the formations of +16 Da and +32 Da products at *m/z* 802.67 and 818.67 were clearly detected, which are corresponding to the mono- and di-epoxidized products, respectively (**Figure 2.3b**). Tandem mass spectrum of the mono-epoxidized product at *m/z* 802.67 clearly shows the presence of two diagnostic ions at *m/z* 618 and 634 with a 16 Da mass shift, which indicates that the double bond is localized at Δ6 position (**Figure 2.4a**). These results demonstrate the feasibility of AC voltage-induced spray formation and electro-epoxidation for double-bond localization in lipids.

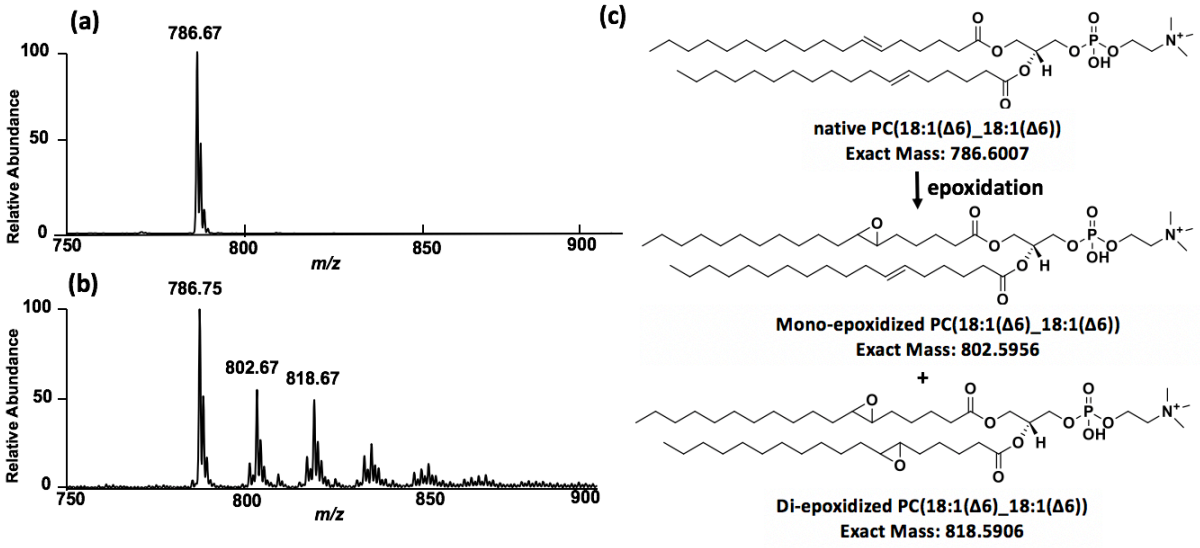

Figure 2.3. Full mass spectra of PC 18:1(Δ6)-18:1(Δ6) solution at (a) high AC voltage (6 kV, peak to peak, square wave, 100 Hz) and (b) low AC voltage (4 kV, peak to peak, square wave, 100 Hz); (c) Scheme of the mono- and di-epoxidation reaction products of PC 18:1(Δ6)-18:1(Δ6). (One mono-epoxidized lipid is shown in the figure.)

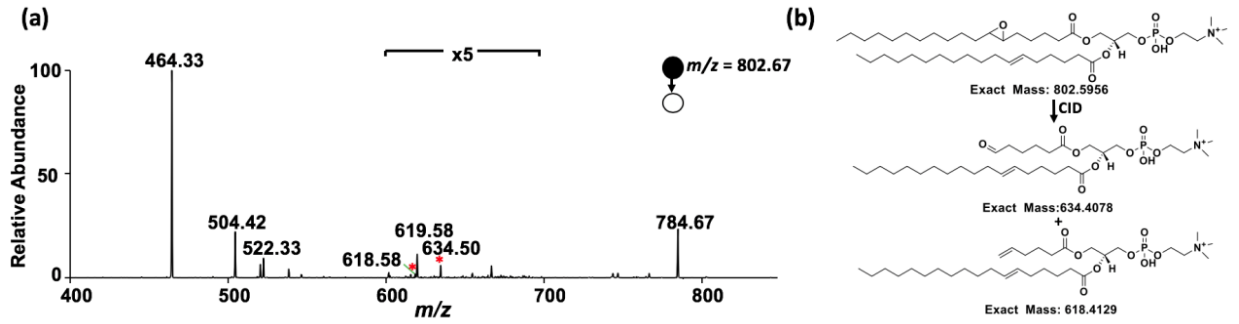

Figure 2.4. (a) Tandem mass spectrum of mono-epoxidized product at *m/z* 802.67, where diagnostic ions (star marked) are observed at *m/z* 618 and 634; (b) Scheme of the fragmentation of mono-epoxidized product.

As a comparison, direct current (DC)-ESI was also tested using an identical solution system. Providing the optimized DC voltage at 1.8 kV in positive ion mode, the epoxidation efficiency was similar to that in AC-ESI (**Figure 2.5**). This experimental result illustrates the epoxidation efficiency is similar using AC induction and DC induction.

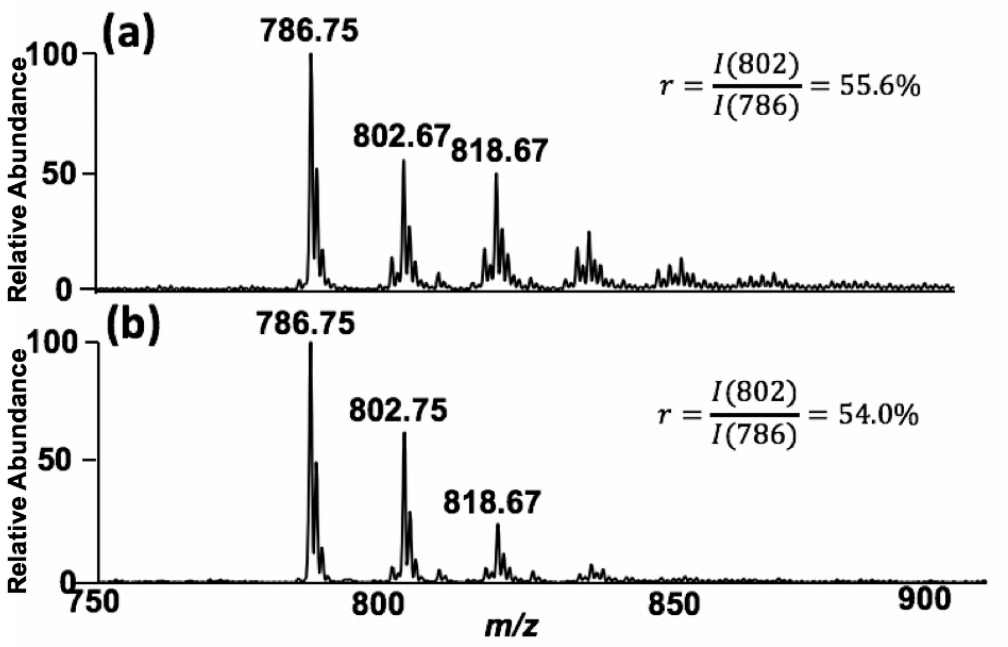

Figure 2.5. Full mass spectra of PC 18:1(Δ6)-18:1(Δ6) electro-epoxidation induced by (a) AC voltage (4 kV, peak to peak, square wave, 100 Hz) and (b) DC voltage (1.8 kV, positive)

To further broaden the range of lipids capable of using electrochemical epoxidation for double-bond localization, negatively-charged lipid was tested using the same AC-ESI set-up. Oleic acid (FA 18:1(Δ9), 20 μM) in acetonitrile/water (80/20, v/v) with 10 mM NH_4Cl was loaded into a nanoESI emitter for electro-epoxidation upon the application of 4.2 kV AC voltage. The formation of epoxidized oleic acid at *m/z* 297.24 was detected (**Figure 2.6**). Two diagnostic ions at *m/z* 155 and 171 of the epoxidized product were observed in the tandem MS spectrum (**Figure 2.7**). The diagnostic peaks have the signature 16 Da mass shift, indicating the double-bond position at Δ9 in oleic acid. These results

demonstrate that AC-ESI can be used for double-bond localization of negatively charged lipids and detection in negative ion mode.

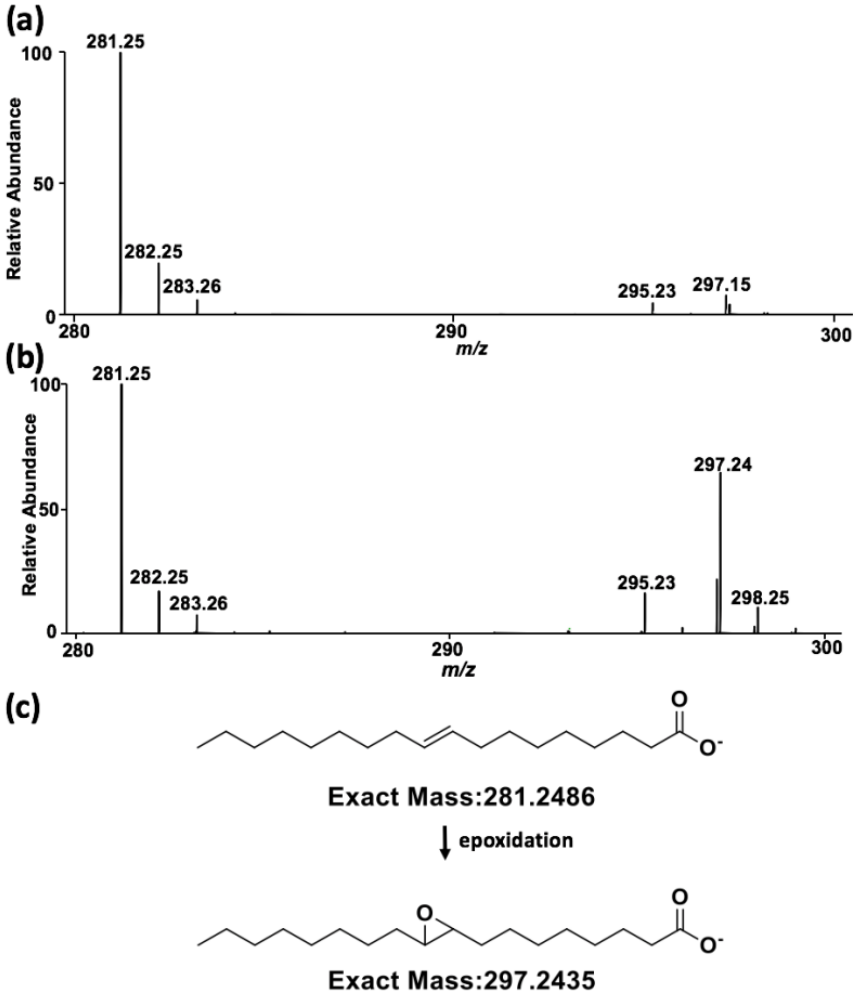

Figure 2.6. Full mass spectra of oleic acid (FA 18:1(Δ9)) at (a) high AC voltage (6 kV, peak to peak, square wave, 100 Hz) and (b) low AC voltage (4 kV, peak to peak, square wave, 100 Hz); (c) Scheme of oleic acid epoxidation.

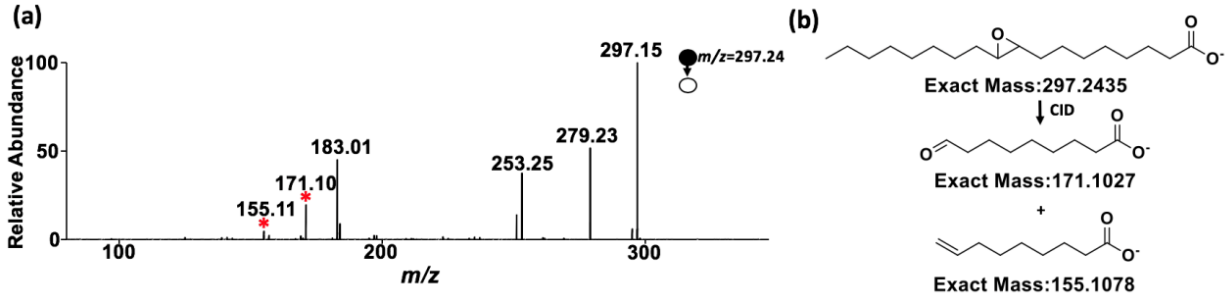

Figure 2.7. (a) Tandem mass spectrum of epoxidized oleic acid at *m/z* 297.24, where diagnostic ions (star marked) are observed at *m/z* 155 and 171; (b) Scheme of the fragmentation of epoxidized product.

2.3.2 Simultaneous Detection of the Double-Bond Locations in Both Positively and Negatively Charged Lipids

With the achievements of double-bond localization for unsaturated lipids in both positive and negative ion modes separately, we further evaluated the application of AC-ESI in simultaneous detection of the double-bond locations in lipids in both ion modes. In the separate experiments, the optimal solvent systems were different when using different ion modes. In positive ion mode, a high concentration of hydrochloric acid was used to protonate lipids, remove sodium adducts and provide the chloride ions required for electro-epoxidation. In negative ion mode, a high concentration of acid would block deprotonation and suppress the lipid detection in negative ion mode. Thus, ammonium chloride was used to provide chloride ions.

In order to perform simultaneous detection of lipids in both ion modes, the solvent

system needs to not only provide enough chloride ions, but also maintain a proper pH for the coexistence of protonated and deprotonated lipid ions. A series of concentrations of hydrochloric acid and ammonium chloride were tested. The optimal condition was found to be a mixture of NH_4Cl (10 mM) and HCl (1 mM) for simultaneous lipid detection in both ion modes.

To perform the experiment of simultaneous detection of lipids in both ion modes, a mixture of PC 18:1(Δ6)-18:1(Δ6) (20 μM) and FA 18:1(Δ9) (20 μM) in acetonitrile/water (80/20, v/v) with 10 mM NH_4Cl and 1 mM HCl was tested using the AC-ESI setup. In both ion modes, the epoxidation peaks with +16 Da mass shift were detected upon the application of 4 kV AC voltage (**Figure 2.8a, b**). The diagnostic ion pairs with a signature 16 Da mass separation were also detected in the tandem mass spectra using CID fragmentation (**Figure 2.8c, d)**.

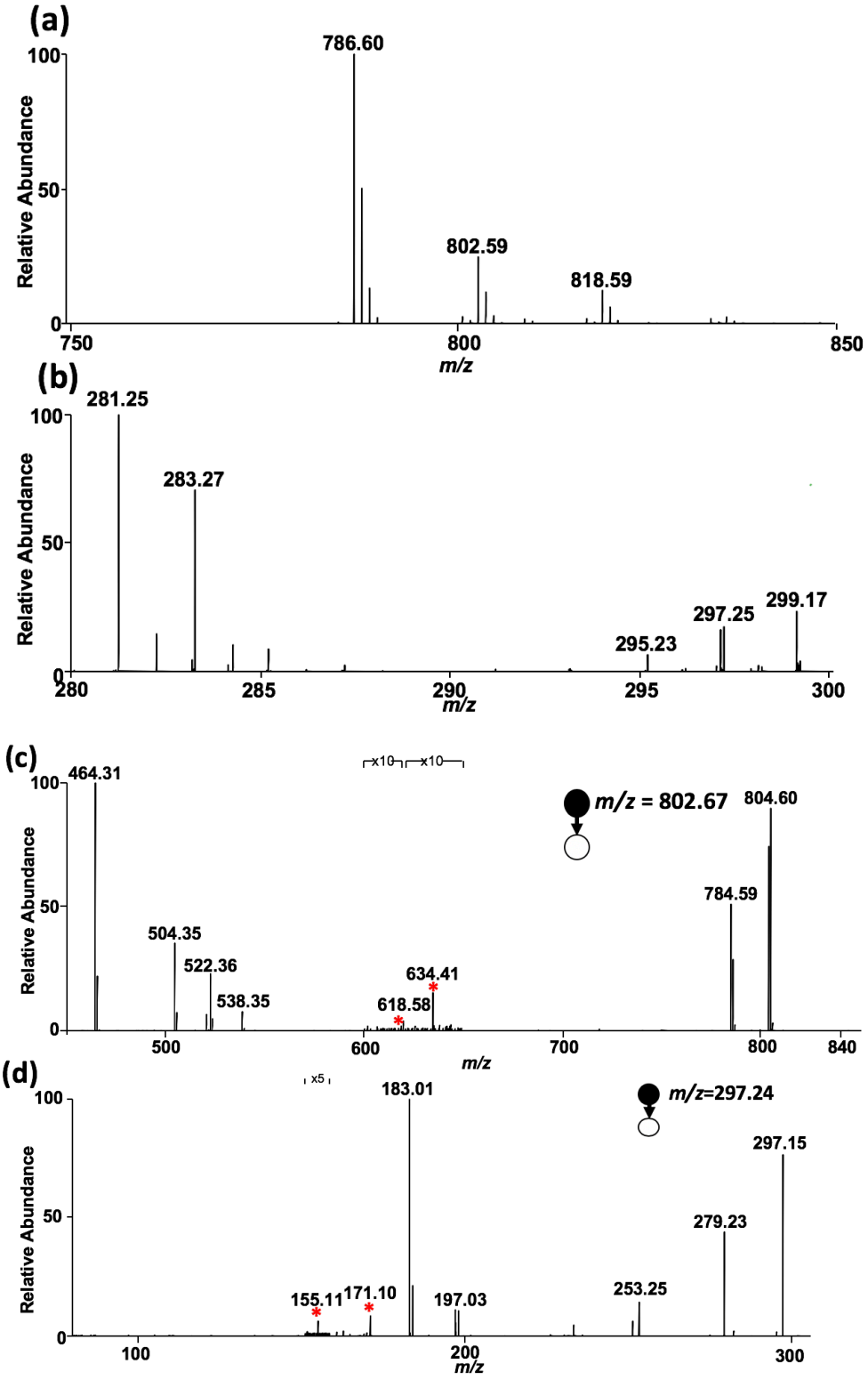

Figure 2.8. Simultaneous detection of epoxidized (a) PC (18:1(Δ6)-18:1(Δ6)) and (b) oleic acid (FA 18:1(Δ9)) in full mass spectra and (c, d) their corresponding tandem mass spectra. Diagnostic ions are labeled with red stars.

2.3.3 Quantification

After the demonstration of double-bond localization capability of unsaturated lipids in both ion modes simultaneously, we further evaluated the application of AC-ESI in quantitative analysis. **Figure 2.9** shows the calibration curve of PC 18:1(Δ6)-18:1(Δ6) and PC 18:1(Δ9)-18:1(Δ9) over concentrations. Two PCs were dissolved in acetonitrile/water (80/20, v/v) with 10 mM NH_4Cl, 1 mM HCl and 50 μM oleic acid. Their diagnostic peak intensity ratios were plotted against their concentration ratios. The diagnostic peaks at *m/z* 634 and 676 were chosen, since another diagnostic peak at *m/z* 618 was shown in the background. The calibration curve shows a good linearity (R^2 = 0.9961). Meanwhile, the limits of detection (LOD) were evaluated for PC 18:1(Δ6)-18:1(Δ6) and FA 18:1(Δ9). The diagnostic fragment ions could be observed with acceptable signal/noise at 1 μM for both lipids (**Figure 2.10**).

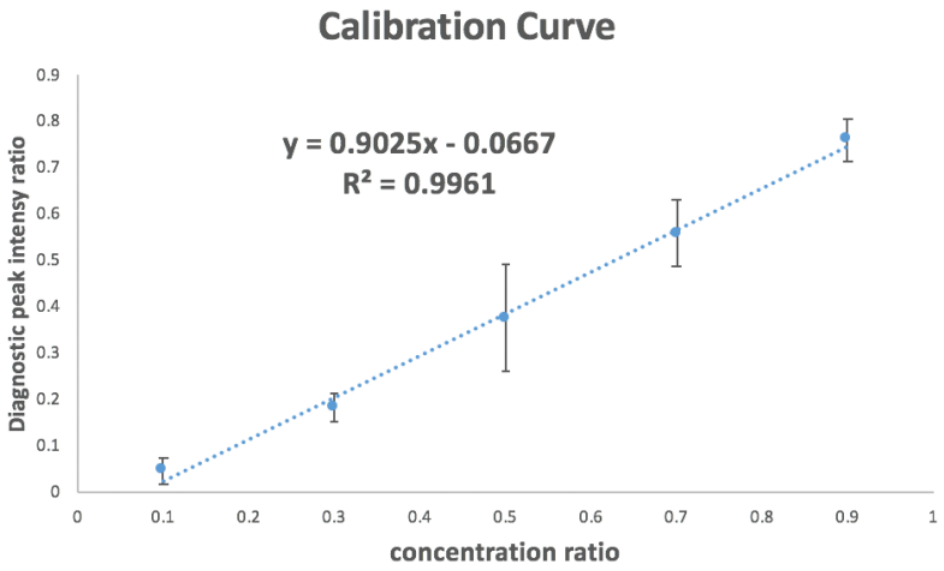

Figure 2.9. Linear relationship between the diagnostic ion intensity ratio (I_{634}/I_{676}) and the concentration ratio ($C_{\Delta6}/C_{\Delta9}$) of double-bond positional isomers PC 18:1(Δ6)-18:1(Δ6) and PC 18:1(Δ9)-18:1(Δ9). The error bar is estimated based on the standard deviation of 3-4 tests.

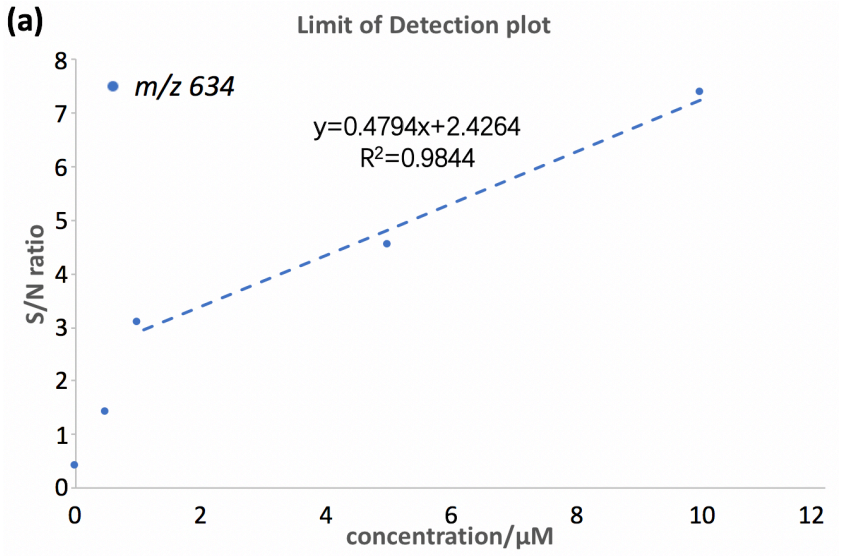

Figure 2.10. Limit of detection plots for (a) diagnostic ion at *m/z* 634 for PC 18:1(Δ6)-18:1(Δ6) and (b) diagnostic ions at *m/z* 155 and 171 for FA (18:1(Δ9)).

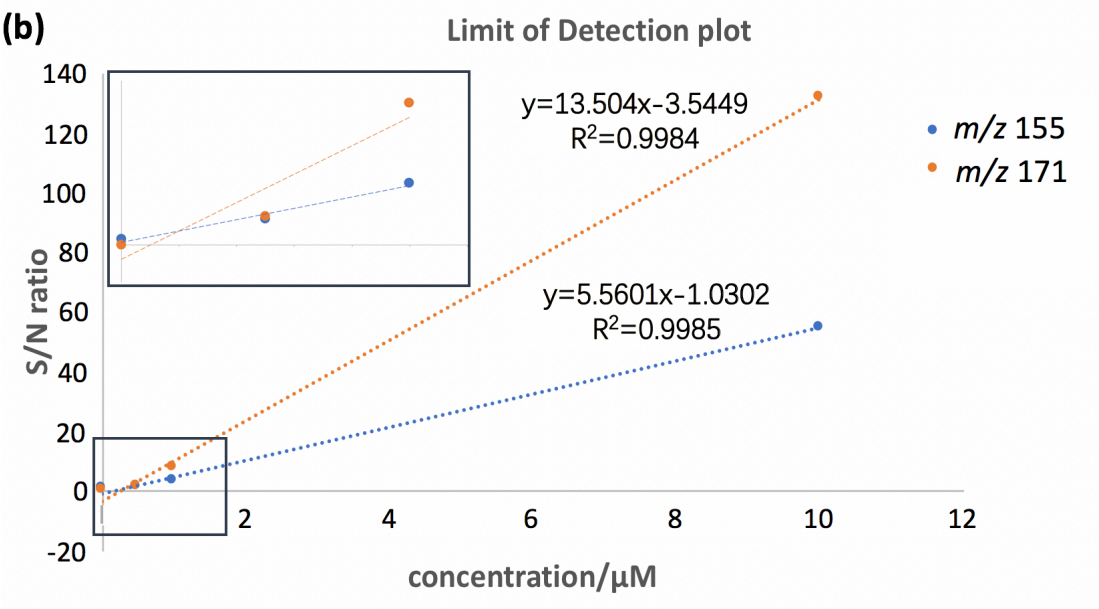

Figure 2.10. Continued.

2.3.4 Analysis of Lipid Extracts of Mouse Brain Using AC-ESI

The lipid extracts were obtained through the Folch method (see Section 2.2.2). We first analyzed lipids before electro-epoxidation. The lipids were mixed with hydrochloric acid solution (10 mM, dissolved in acetonitrile/ water (80/20, v/v)). When 6 kV AC voltage was applied, only protonated lipids were detected (**Figure 2.11a**). The high resolution mass spectrum coupled with tandem mass spectrum provides accurate mass as well as lipid fragments. Lipid species including head group isomers and chain length isomers were characterized through signature head group loss and fatty acyl chain loss (see **Appendix**). The identified head group isomers and chain length isomers are listed in

Table 2.1 and **Table 2.2**, respectively.

Upon the application of 4 kV AC voltage, the pattern of the mass spectrum switched quickly, and epoxidation peaks with +16 Da mass shift were observed (**Figure 2.11b, c**). Tandem mass spectra were obtained through the CID over these epoxidized peaks and the double-bond locations were identified through the diagnostic ion pairs with a signature 16 Da mass shift (See **Appendix**). The phenomenon of double-bond positional isomer exists in most detected unsaturated lipids in the brain sample. They were identified and listed in **Table 2.3**.

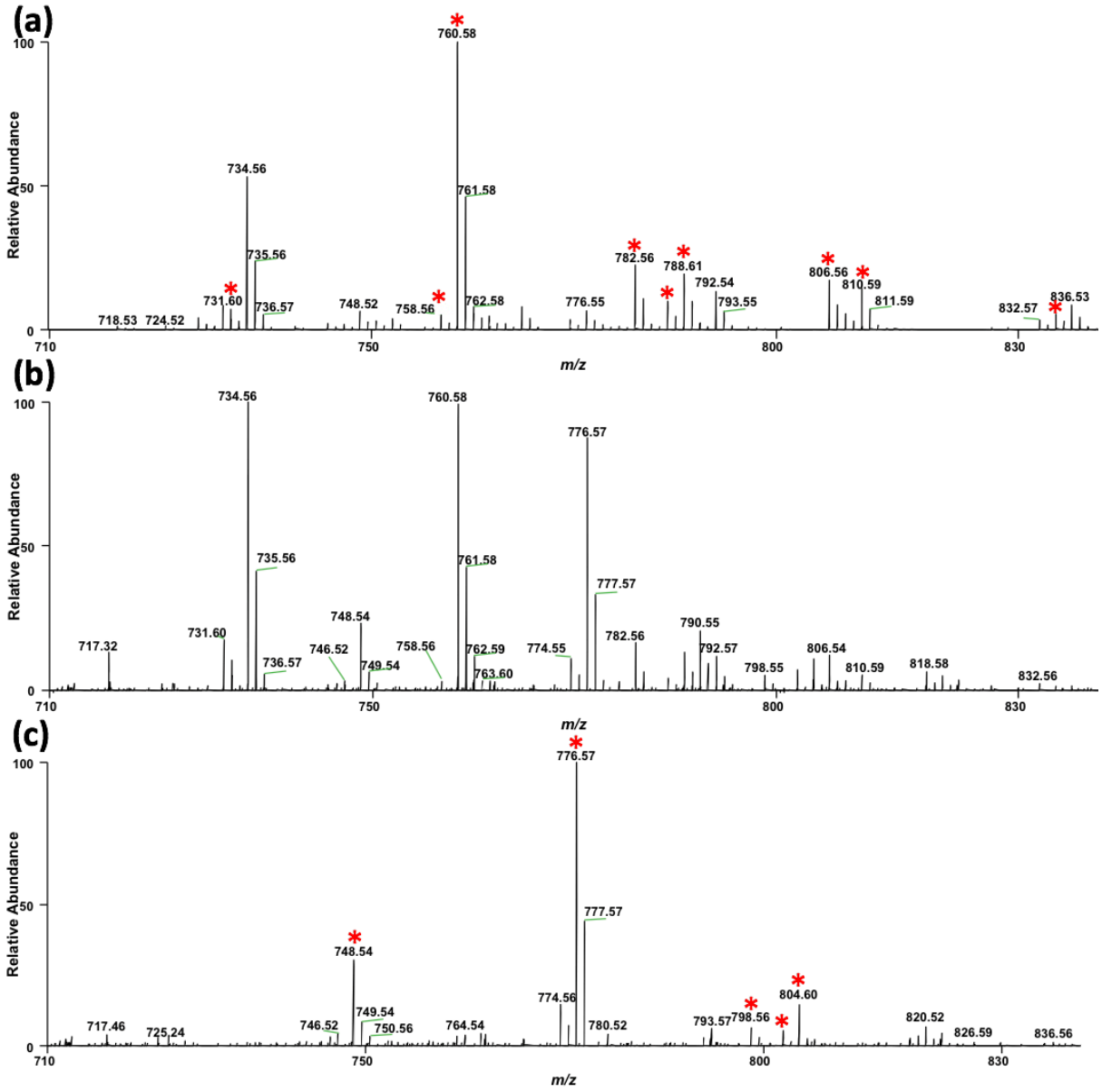

Figure 2.11. Full mass spectra of the lipid extracts from mouse brain obtained at (a) high AC voltage (6 kV, peak to peak, square wave, 100 Hz), and (b) low AC voltage (4 kV, peak to peak, square wave, 100 Hz); (c) mass spectrum after background subtraction which indicates the epoxidation peaks with +16 Da mass shift. Identified native phospholipids and epoxidized phospholipids are labeled in (a) and (c), respectively.

Table 2.1 Identified head group isomers from the mouse brain lipid extract

Measured Mass	Tentative Ion Identification	Theoretical mass (Monoisotopic)	Mass error (ppm)	Head group loss MS^2 fragment Ions
732.5448	PC(32:1)	732.5538	-12	673(-59),549(-183)
	PE(35:1)	732.5538	-12	591(-141)
758.5599	PC(34:2)	758.5694	-12	699(-59), 575(-183)
	PE(37:2)	758.5694	-12	617(-141)
	PS(p-35:2)	758.5336	+36	573(-185)
760.5755	PC(34:1)	760.5851	-12	577(-183)
	PE(37:1)	760.5851	-12	619(-141)
782.5595	PC(36:4)	782.5694	-12	723(-59), 599(-183)
	PE(39:4)	782.5694	-12	641(-141)
786.5906	PC(36:2)	786.6007	-12	727(-59), 603(-183)
	PE(39:2)	786.6007	-12	743(-43), 645(-141)
	PS(P-37:2)	786.5634	+36	601(-185)
788.6065	PC(36:1)	788.6164	-12	729(-59), 605(-183)
	PE(39:1)	788.6164	-12	745(-43), 647(-141)
	PS(P-37:1)	788.5800	+33	603(-185)
806.5590	PC(38:6)	806.5694	-12	747(-59), 623(-183)
	PE(41:6)	806.5694	-12	763(-43), 665(-141)
810.5905	PC(38:4)	810.6007	-12	751(-59), 627(-183)
	PE(41:4)	810.6007	-12	669(-141)
	PS(P-39:4)	810.5649	+33	625(-185)
834.5905	PC(40:6)	834.6007	-12	775(-59), 651(-183)
	PE(43:6)	834.6007	-12	791(-43), 693(-141)
	PS(39:0)	834.6219	-37	649(-185)

Table 2.2. Identified chain length isomers from the mouse brain lipid extract

Parent ion Mass (Monoisotopic)	Tentative ion identification	Chain Length isomers MS^2 Fragment ions
732.5448	PC(32:1)	PC(16:1/)-476,494
		PC(16:0/)-478,496
758.5599	PC(34:2)	PC(16:1/)-476,494
		PC(16:0/)-478,496
		PC(18:2/)-502,520
		PC(18:1/)-504,522
760.5755	PC(34:1)	PC(16:0/)-478,496
		PC(18:1/)-504,522
782.5595	PC(36:4)	PC(16:0/)-478,496
		PC(20:4/)-526,544
786.5906	PC(36:2)	PC(16:0/)-478,496
		PC(18:1/)-504,520
		PC(20:2/)-530,548
788.6065	PC(36:1)	PC(16:0/)-478,496
		PC(18:1/)-504,522
		PC(18:0/)-506,524
		PC(20:1/)-532,550
806.5590	PC(38:6)	PC(16:0/)-478,496
		PC(20:6/)-522,540
		PC(22:6/)-550,568
810.5905	PC(38:4)	PC(16:0/)-478,496
		PC(18:0/)-506,524
		PC(20:4/)-526,544
		PC(22:4/)-554,572
834.5905	PC(40:6)	PC(16:0/)-478,496
		PC(18:1/)-504,522
		PC(18:0/)-506,524
		PC(22:6/)-550,568
		PC(24:6/)-578,596

Table 2.3. Identified double-bond positional isomers from the mouse brain lipid extract

Parent ion mass (Monoisotopic)	Tentative ion identification	Theoretical mass	Mass error (ppm)	Double-bond positional isomers MS^2 diagnostic ions
776.5700	PC(34:1)	776.5805	13.5	PC(16:0_18:1(Δ6))-592,608
				PC(16:0_18:1(Δ9))-634,650
				PC(16:0_18:1(Δ11))-662,678
748.5389	PC(32:1)	748.5492	13.8	PC(16:0_16:1(Δ9))-634,650
				PC(16:0_16:1(Δ12))-674,690
804.6010	PC(36:1)	804.6118	13.4	PC(18:0_18:1(Δ9))-662,678
				PC(18:0_18:1(Δ11))-690,706
				PC(18:0_18:1(Δ12))-714,730
798.5534	PC(36:4)	798.5649	14.4	PC(16:0_20:4(Δ5, Δ8, Δ11, Δ14))-618,634/658,674
				PC(18:2(Δ12, Δ15)_18:1(Δ12, Δ15))-700,716/740,756
802.5854	PC(36:2)	802.5962	13.5	PC(18:1(Δ6)_18:1(Δ6))-618,634
				PC(18:1(Δ9)_18:1(Δ9))-660,676
				PC(18:1(Δ12)_18:1(Δ12))-688,704
				PC(18:0_18:2(Δ9, Δ12))-662,678/688,704

2.4 Discussion

The experimental results demonstrate the feasibility of AC-ESI for lipid double-bond localization in both positive and negative ion modes. The electro-epoxidation efficiencies of AC-ESI and DC-ESI are comparable when optimal solvent system and voltage are applied. The diagnostic peaks are clearly detected with 16 Da signature mass difference in tandem mass spectrum. Through the control of concentrations of ammonium chloride and hydrochloric acid in lipid solution, we are able to perform lipid detection with double-bond positional isomer differentiation for both phospholipids and fatty acids in a single experimental run.

The electro-epoxidation is initiated in the positive half work cycle for lipid ions regardless of polarities, and the epoxidized lipid cations and anions are detected at different half work cycles, respectively.

The quantification study shows the great linearity of intensity ratios of double-bond positional isomers over concentrations with good limit of detection. The results shows that AC-ESI method allows quantitative analysis of lipids. In complex sample analysis, the lipid extracts from mouse brain were used and phospholipids are identified with differentiation of head group isomers, chain length isomers and double-bond positional isomers.

The current methods that can detect double-bond localization in both positive and

negative modes usually require additional reagents, extra apparatus or multiple steps.[45,73] Compared to them, the AC-ESI lipid analysis method demonstrated in this section has the following advantages: i) no requirement for external apparatus, which makes it compatible with mass spectrometry imaging technique (future project); ii) controllable epoxidation induced by an inherent electrochemical reaction, which allows the comparison between native and epoxidized lipids in a single run, and simplifies the workflow for complex sample analysis; iii) low sample consumption enabled by the fact that lipids in both ion modes can be detected simultaneously. The unique capability of simultaneous localization of lipid double bonds in both positive and negative ion modes and the convenient setup enables its wide application in a broad range of biological systems.

3. DISCOVERY OF REGION-SPECIFIC LIPIDS IN MOUSE BRAIN AND BIOMARKERS FOR ALCOHOLISM USING DESORPTION ELECTROSPRAY IONIZATION-MASS SPECTROMETRY IMAGING

3.1 Introduction

Alcoholism is a primary, chronic relapsing disease of brain reward, motivation, memory and related circuitry.[74] Many studies have shown that excessive ingestion of alcohol results in the alteration of lipid metabolism, such as lipolysis inhibition and free fatty acid level decrease.[75-77]

Animal and human studies have suggested that dorsal striatum plays a crucial role in habitual learning and memory processes that may underlie compulsive alcohol administration.[78,79] Several research groups have reported that metabolic pathways were modified upon the exposure of dorsal striatal neurons to ethanol, such as the activation of the Fyn gene and phosphorylation of NR2B subunit.[80,81] Moreover, these effects were not observed in the structurally related ventral striatum region, which indicated that the modifications were region-specific.[80] The subtle metabolism differences in specific regions can be lost if a homogenate of tissue is used for analysis. Thus, an analytical technique that can provide spatial information of the mouse brain is necessary for the study of lipid change after the intake of alcohol.

Mass spectrometry imaging is a powerful tool that allows untargeted investigations into the spatial distribution of molecular species. Through the combination of structural identification and visualization of different species in space, MSI has become a valuable technique for lipid study in mouse brain. Histochemical staining can be performed after MSI to provide morphology information.[82]

Desorption electrospray ionization-MSI is an ambient MSI technique that is specifically applicable to the investigation of lipids, and is chosen in this section to study lipid changes in the mouse brain. The ambient operation environment with no sample preparation and the soft ionization in DESI-MSI allow maintaining sample morphology while obtaining metabolite information from the sample surface. DESI-MSI has been applied in biomarker discovery for disease diagnosis based on lipid profiles.[82] The presence of specific lipid species is characterized by MS analysis followed by multivariate statistical analysis. In this section, we applied DESI-MSI to find molecular markers of brain regions and to discover lipid biomarkers for alcoholism in mouse brain.

3.2 Materials and Methods

3.2.1 Biological Sample Preparation

Female mice (~8 weeks old) were randomly assigned and counterbalanced based on weight to the experimental group and the control group. Before breeding, mice were housed under a 12 hour light/dark cycle with food and water available *ad libitum.* The

control group had free access to tap water only and the alcohol-drinking group had access to both water and a 20% alcohol solution (v/v in tap water). An intermittent alcohol access was employed to establish a high level of alcohol consumption in the experimental group. Briefly, female mice were given 24-hour access to both alcohol solution and tap water every other day for a week. This paradigm has been reported by other research to induce high levels of alcohol intake, up to 30 g/kg/d at 20% v/v in female mice.[83]

Striatal slice was prepared using the following protocol. Mice were transferred from the vivarium to the procedure room twenty-four hours after the last alcohol-drinking session. Mice were anesthetized with 0.5% isoflurane. Minimum optimal cutting temperature (OCT) solution was used to attach the cerebellum of the brain tissue to the mounting plate before sectioning the mouse brain. Coronal sections of the brain (~10 μm) were sliced using a vibratome (VT1200s; Leica Biosystems, Inc., Buffalo Grove, IL). Serial sections were made and directly thaw mounted onto a microscope glass slide (Eisco Scientific LLC, Victor, NY). All procedures mentioned above were performed in the lab of Prof. Jun Wang (Institute for Neuroscience, TAMU). The sections were stored at -80 °C and dried in a vacuum desiccator for 15 minutes prior to MSI analysis.

3.2.2 Mass Spectrometry

3.2.2.1 Ion Source

The DESI stage consists of a DESI emitter, a high voltage power supply, a sheath gas pipeline, and a programmable moving stage with glass slide mount. The DESI stage is coupled with a mass spectrometer using a customized sniffer inlet.

The homemade DESI emitter was built using a fused silica capillary (50 μm inner diameter, 150 μm outer diameter, Polymicro Technologies LLC) as an inner capillary for solvent delivery and a coaxial fused silica capillary (250 μm ID, 360 μm OD, Polymicro Technologies LLC) as an outer capillary for sheath gas delivery. The inner capillary extended approximately 0.5 mm outside the outer capillary. The emitter was connected with a sheath gas tank through a Swagelok T union and the inner capillary was connected with the syringe through another union. Plastic tubing delivered the compressed nitrogen to the Swagelok T at 160 psi. Solvent was pumped from the syringe with a microprocessor syringe pump (Harvard Apparatus Model 22, Holliston, MA). High voltage was supplied by the built-in high voltage power supply from the LTQ-XL mass spectrometer. Finally, the DESI emitter was fixed on the extended arm of the DESI stage (Prosolia Scientific, Indianapolis, IN). **Figure 3.1** shows the configuration of DESI stage with a homemade DESI emitter.

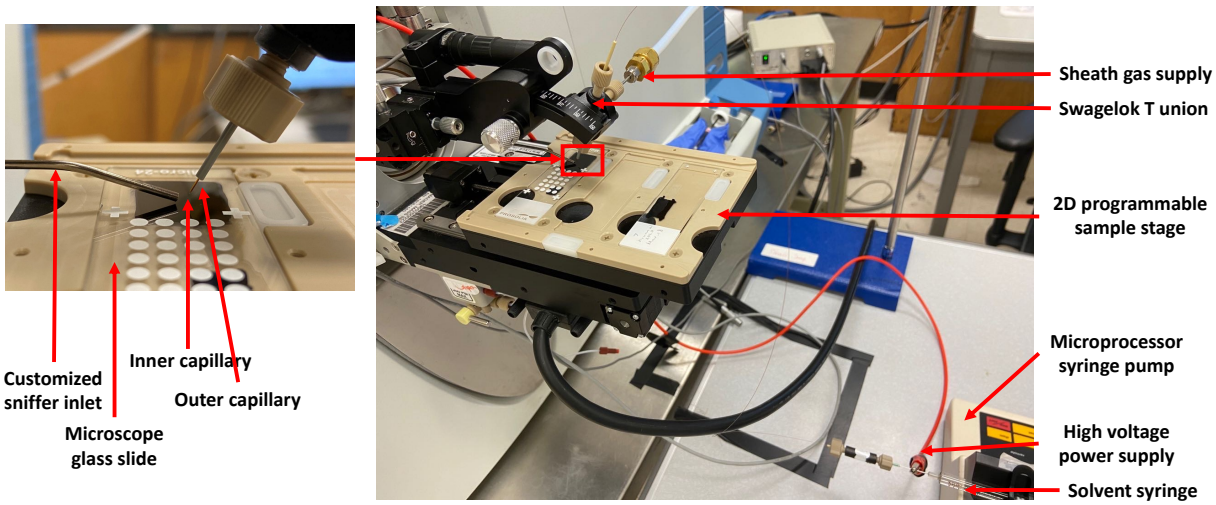

Figure 3.1. Configuration of homemade DESI ion source.

All parameters were optimized for tissue scanning. The distance between the DESI emitter tip and the sample surface was approximately 1 mm. The distance of the emitter tip to the mass spectrometer inlet was approximately 4 mm. The DESI emitter angle was 55 degrees relative to the tissue surface. All tissue sample sections were held in the programmable 2D sample stage, which communicated with the LTQ XL mass spectrometer to raster the tissue sample and to obtain mass data for each pixel. The pixel size was set as 100 μm by 100 μm. The mass spectrometer was operated in negative ion mode with 3.5 kV voltage applied on the syringe needle. Acetonitrile: dimethylformamide (80/20, v/v) was chosen as the solvent system sprayed at a flow rate of 2 μL/min.

3.2.2.2 Mass Analyzer

A linear Ion Trap (LTQ) Mass Spectrometer (Thermo Fisher Scientific Inc.) was used

as the mass analyzer for DESI-MSI.

The following MS parameters were used for data acquisition. Samples were ionized in the negative ion mode and the spray voltage was set at 3.5 kV. In negative ion mode, tube lens voltage was at -101.46 V, and capillary temperature was set to be 275°C. Full MS scans were acquired at *m/z* 100-1000. Two microscans were used for full MS scans with the maximum injection time of 200 ms. Automatic gain control (AGC) was turned on.

3.2.3 Data Analysis for MSI

In order to construct two-dimensional images from raw MS data, MSiReader (msireader.wordpress.ncsu.edu) was used.[84] MSiReader is an open-source vendor-neutral MATLAB application to view and perform data analysis of MSI data. Region-specific data sets were extracted through MSiReader.

As for the statistical analysis, Metaboanalyst (www.metaboanalyst.ca) was used for data analysis and biomarker discovery.[85] Metaboanalyst is a free, user-friendly and easily accessible tool for high-throughput metabolomics data analysis. Statistical analysis and biomarker discovery were explored using the region-specific datasets in Metaboanalyst.

3.3 Results and Discussion

3.3.1 Mass Spectra Obtained from DESI-MSI

Mass spectra of mouse brain tissue collected from both experimental and control groups were acquired by DESI-MSI with the mass range set from *m/z* 100-1000. Lipid species in

brain tissues including fatty acids, monoacylglycerols and phospholipids were observed in this *m/z* range. A typical single-scan mass spectrum is shown in **Figure 3.2**. The MS spectrum was dominated by the lipid ion at *m/z* 834.67 (tentatively identified as phosphatidylserine (40:6)). Major peaks in the spectrum include fatty acids (*m/z* range from 200-400) and other phospholipids (*m/z* range from 700-900). The inset of the total ion chronogram shows the strong ion intensities from the brain sample region over the background region when the DESI probe scans a line on the tissue. The background signal is less than 1% of the signal in the spectrum of brain sample.

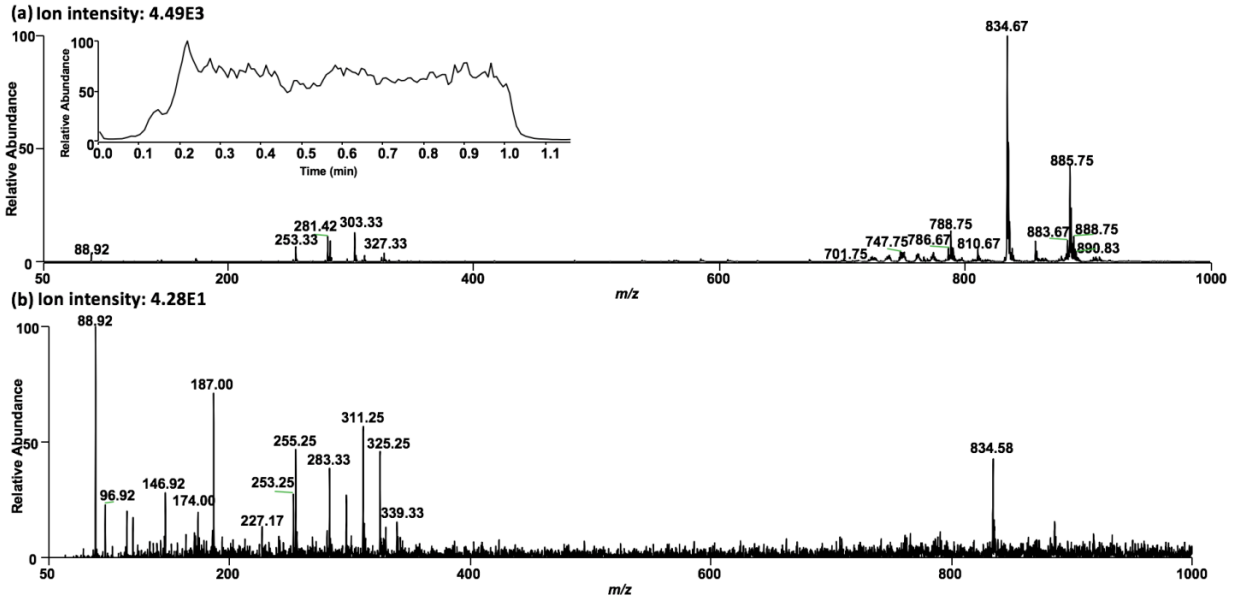

Figure 3.2. Mass spectra obtained from DESI-MSI of (a) sample region and (b) background region. The inset total ion chromatogram (TIC) shows the strong MS signal of the brain sample compared with the background signal.

3.3.2 Region Identifications

To perform the region-specific data analysis in the later step, images from both experimental and control groups were used for region identification. The mass spectrometry images were reconstructed using MSiReader. The .iMZML document converted from the raw documents contains the required meta-information with smaller document size and faster loading speed. In reconstructed images, the spots per line were decided by the number of mass spectra obtained in each line and the number of lines was determined by the number of the raw documents in one sample. The heatmap of each *m/z* value was reconstructed by showing the spatial distribution of metabolite of specific *m/z* value.

The *m/z* window is set at 0.5 Da considering the resolution power of mass analyzer. For some of the images obtained, there is a clear boundary between the tissue region and the background region. Moreover, the distributions of some lipids show specific patterns within the brain section region, which can be used for region identification (**Figure 3.3**). For example, the lipid at *m/z* 327.5 (tentatively identified as docosahexaenoic acid (fatty acid (22:6))) concentrated in the two round small regions in the MSI image.

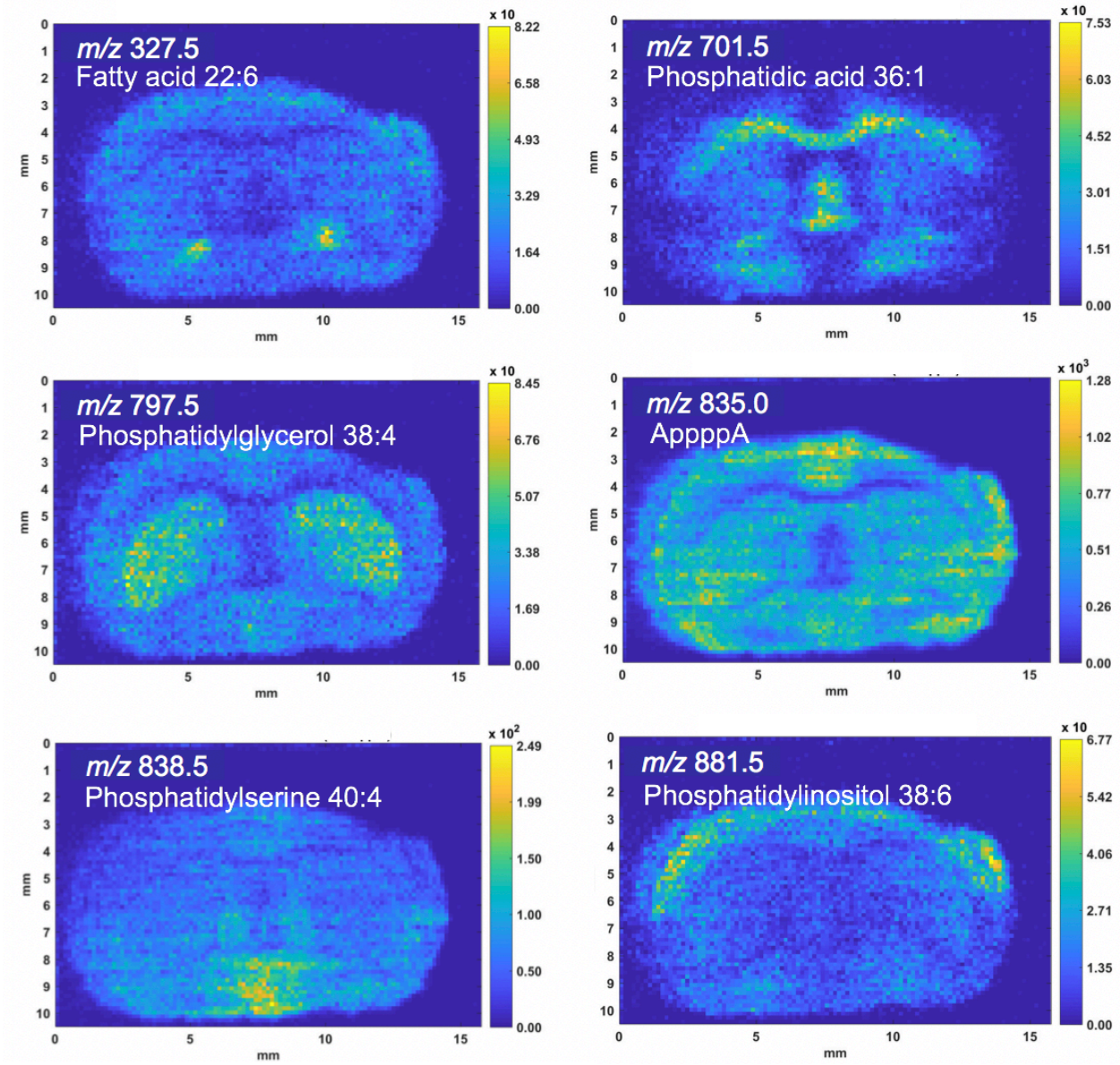

Figure 3.3. DESI-MSI images showing representative *m/z* values that are specific to mouse brain regions. (Image credit: Allen Institute.)

Among all the regions in the brain section, the distribution of *m/z* 701.5 (tentatively identified as phosphatidic acid (36:1)) shows a unique shape that is aligned with the distribution of fiber tracts in the coronal sections of the brain. Fiber tracts are a bundle of

nerve fibers connecting nuclei of the central nervous system with unique shapes within the coronal sections of mouse brain and a broad existence in different sections. Herein, fiber tracts were used for the alignment between mass spectrometry images and the standard anatomical histochemical stain images of a P56 mouse from Allen Brain Reference Atlases.[86] Through the alignment of the MSI image with the staining image using the molecular marker at *m/z* 701.5, the relative location of different brain regions within the tissue section can be determined accordingly (**Figure 3.4**).

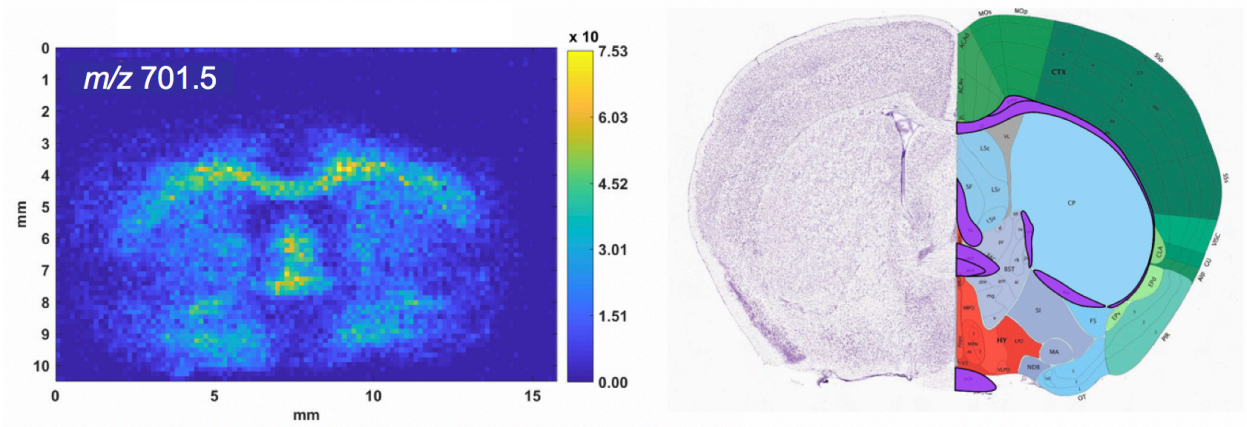

Figure 3.4. (Left) The MSI image of the biomarker at *m/z* 701.5 and (right) standard anatomical histochemical stain image (fiber tracts were labelled in purple, Image credit: Allen Institute.) were used for image overlay.

Several other regions including magnocellular nucleus, dorsal striatum region and brain stems were successfully localized through the distribution of certain biomarkers and their relative location as fiber tracts (**Figure 3.5**).

Conventionally, the brain region identifications were performed through the adjacent tissue slice staining or post-analysis staining, which is time-consuming and requires larger sample size for both experiments.[82] The simple region identification method illustrated above makes the use of the unique shape of fiber tracts in coronal brain sections and no histochemical staining is required for preliminary region identification in MSI study.

Specifically, the dorsal striatum region, the region-of-interest (ROI) for alcoholism study, was successfully identified through the simple region identification method, which allows the region-specific biomarker discovery of alcoholism at an early-stage.

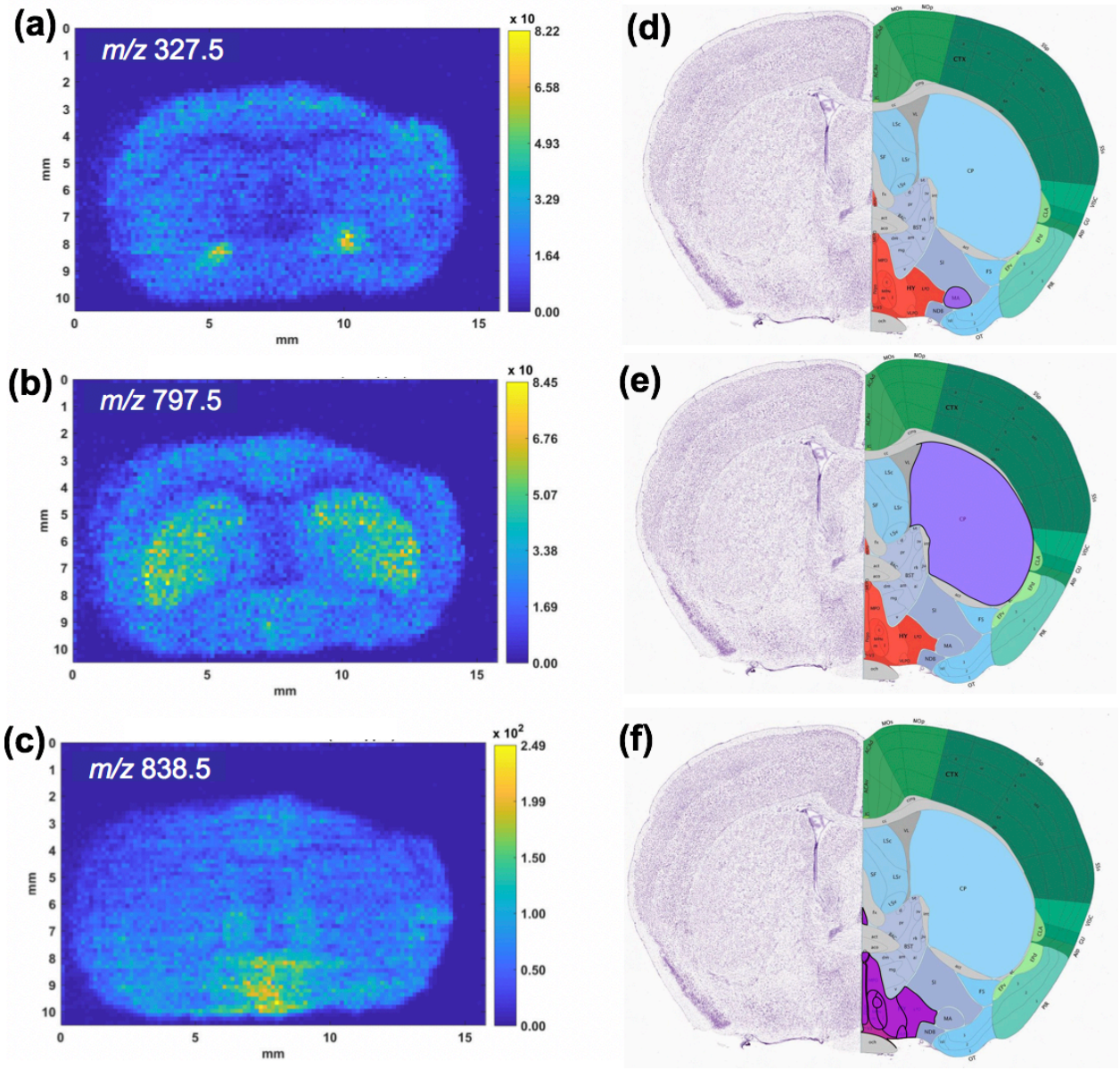

Figure 3.5. (Left) The MSI image of the biomarker at (a) *m/z* 327.5 (tentatively identified as fatty acid (22:6)) (b) *m/z* 797.5 (tentatively identified as phosphatidylglycerol (38:4)) (c) *m/z* 838.5 (tentatively identified as phosphatidylserine (40:4)) and (right) standard anatomical histochemical stain images of (d) magnocellular nucleus, (e) dorsal striatum region, (f) brain stems (all labelled in purple, Image credit: Allen Institute.).

3.3.3 Statistical Analysis and Biomarker Discovery

The dorsal striatum region was chosen as the ROI and the mass spectrum data within the dorsal striatum region were binned and exported for further analysis via MSiReader. The bin width was set at 0.1 Da considering the resolving power of the mass analyzer and the analysis capability of Metaboanalyst.

The dataset contained mass information from eight experimental groups and seven control groups. Several algorithms were tested for classification including partial least squares – discriminant analysis (PLS-DA), sparse partial least squares – discriminant analysis (sPLS-DA), and significance analysis of microarrays (SAM), etc.

PLS-DA is a supervised algorithm for the group classification. PLS-DA uses multivariate regression techniques to extract the information that can predict the class membership (Y) via linear combinations of original variables (X). Herein, the best classifier can be built using 5 components with R^2 value around 0.98 (R^2 value greater than 0.67 indicates a high predictive accuracy.[87]) and prediction accuracy around 70% (**Figure 3.6a**). A good separation was observed in the 3D scores plot as well (**Figure 3.6b**). Moreover, the potential biomarker was identified through the variable importance in projection (VIP) scores, which are a weighted sum of squares of the PLS loadings considering the amount of explained Y-variation in each dimension. The biomarker at *m/z* 841.83 was identified due to its highest VIP score shown in **Figure 3.6c**.

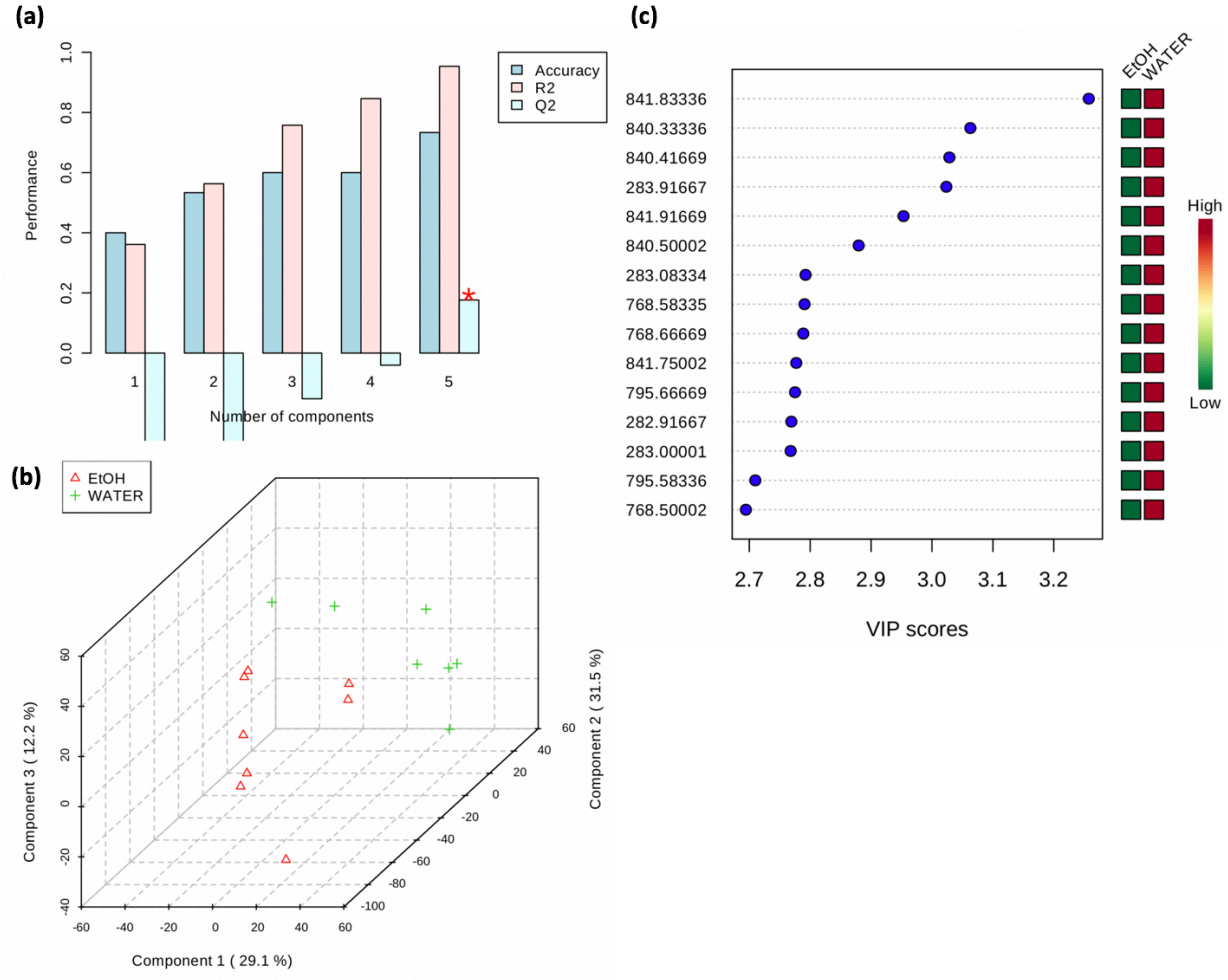

Figure 3.6. Group classification results using PLS-DA. (a) PLS-DA classification using different number of components. The red star indicates the best classifier;(b) 3D scores plot between the selected principle components; (c) Important features identified by PLS-DA. The colored boxes on the right indicate the relative concentrations of the corresponding metabolite in each group under study.

SAM is a well-established statistical method for the identification of expressed genes in microarray data analysis. Previous articles has also reported its applications in MS data for quantitative analysis.[88] A significance score to each variable is assigned based on its

change relative to the standard deviation of repeated measurements in SAM. For a variable with scores greater than an adjustable threshold, its relative difference is compared to the distribution estimated by random permutations of the class labels. Through SAM, only one variable at *m/z* 841.83 was identified as the important features (**Table 3.1**), which also shows the potential for lipid at *m/z* 841.83 as the biomarker for alcoholism group identification.

Table 3.1. Important features identified by SAM

	Peaks (mass)	d.value	stdev	rawp	q.value
1	841.83336	1.6982	0.34205	0.00037694	0.99997

Based on the statistical analysis results mentioned above, potential biomarker at *m/z* 841.8 (tentatively identified as triacylglycerol 51:3) was identified and has the potential to differentiate alcoholism brain tissue samples from the normal samples. Meanwhile, robust biomarkers will be highly likely to be discovered given a larger sample size. The functions of the biomarkers will be studied in the context of the metabolic pathway, and their relationships with the pathogenesis process induced by alcoholism will also be investigated in the future studies.

4. IMPROVEMENT OF SENSITIVITY AND SPECIFICITY IN DETECTION OF 2-ARACHIDONOYLGLYCEROL USING CHEMICAL DERIVATIZATION

4.1 Introduction

2-Arachidonoylglycerol (2-AG) is a unique monoacylglycerol identified as the endogenous ligand for the cannabinoid CB1 and CB2 receptor.[89,90] 2-AG possesses the binding activity to cannabinoid receptors and exhibits a variety of cannabimimetic activities. For example, in neuroblastoma cells, a trace amount of 2-AG, as little as 0.3 nM, can induce a rapid increase in the intracellular free calcium ion concentration through a CB1 receptor-dependent mechanism.[91]

Despite the increasing attention towards 2-AG, direct detection of 2-AG using mass spectrometry is still challenging due to its low abundance and low ionization efficiency in biological samples. The concentration of 2-AG is around 0.34 nmol/g in frozen rat brain and the ionization efficiency of the diol group is low.[92] Another problem in the direct detection of 2-AG is the co-existence of a hydroxyl-positional isomer, 1-arachidonoylglycerol (1-AG).[93] Currently, liquid chromatography-tandem mass spectrometry (LC-MS/MS) is commonly used for 2-AG detection because liquid chromatography can readily separate 1-AG and 2-AG and relieve the matrix effect from the tissue sample.[93,94] However, the requirement for internal standards and time-

consuming steps limit its wide application such as 2-AG imaging studies.

An efficient method to overcome the problems mentioned above is through derivatization. Appropriate derivatization can improve detection sensitivity and resolve isomers. When being used for low-abundance lipid detection, chemical derivatization can also increase the specificity by having different diagnostic fragments from derivatized parent ions.

Various methods have been demonstrated in lipid derivatization, including silylation, alkylation and acylation.[95,96] Appropriate derivatization methods should be selected based on the nature of lipids, the detection platform and the research interest, since no universal method can work in all situations. In this section, the chemical derivatization method using phenyboronic acid for 2-AG detection is developed. The detection specificity of 2-AG was improved compared to the direct protonation, and the feasibility of the method was demonstrated in a complex brain sample.

4.2 Materials and Methods

4.2.1 Lipid Extraction Method

The Folch method was used in 2-arachidonoylglycerol extraction.[72] Multiple solvent systems were tested for comparison and acetonitrile was chosen because it is MS friendly and has a high extraction efficiency. The mouse brain sections were dried in a vacuum desiccator for 15 min. Two sections were transferred from the glass slides into 200 µL

acetonitrile. The mixture was homogenized using a mini homogenizer for 6 minutes until there are no observable chunks of tissues. The mixture was rested until an apparent separation was seen. Syringes and 0.22 μm pore size syringe filters were used to transfer the supernatant. The extraction process using acetonitrile was repeated for 3 times. Combined supernatant from three extractions was centrifuged for 5 minutes at 4500 rpm. The supernatant was collected and used for further analysis.

4.2.2 Mass Spectrometry

4.2.2.1 Ion Source

Single-channel borosilicate capillary tubes (0.86 mm I.D. and 1.5 mm O.D., #1B160-6, World Precision Instruments, Sarasota, FL) were used for nanoESI emitter fabrication. The nanoESI emitters were produced using a P-1000 Flaming/Brown micropipette puller (Sutter Instrument Company Co., Novato, CA).

The following parameters were used for nanoESI emitter fabrication. The HEAT value was set to be 520 with a ramp value of 490. PULL value was set at 0 and the VELOCITY value was set to be 20 with TIME value at 250 and PRESSURE value at 500. Emitter tip geometries were characterized under an optical microscope. The image of a nanoESI tip is shown in **Figure 4.1**.

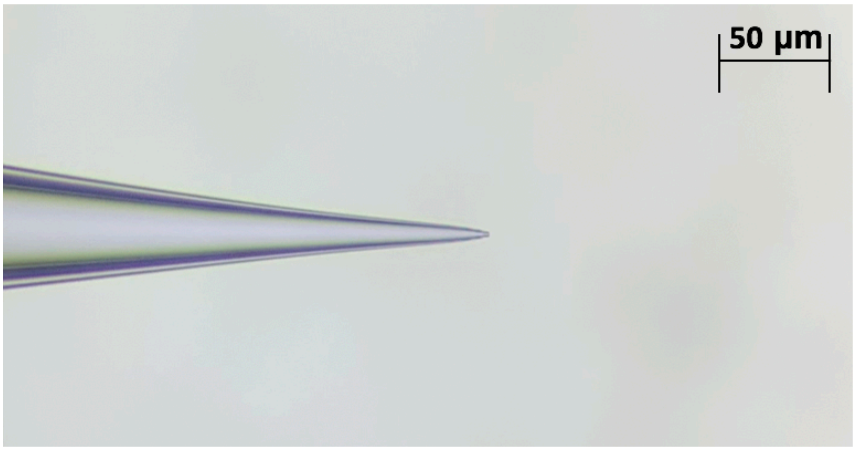

Figure 4.1. The optical image of a nanoESI emitter. The average orifice size is estimated to be 2 µm.

4.2.2.2 Mass Analyzer

LTQ-Velos Pro-Orbitrap (Thermo Fisher Scientific Inc.) was the mass analyzer used in this study. The following parameters were used for data acquisition. Capillary temperature 275 °C, S-lens RF level 67.6% in positive ion mode, and capillary temperature 275 °C, S-lens RF level 60% in negative ion mode, maximum injection time 500 ms and 1 microscan for each individual scan, mass resolution at 60,000. Full MS scans were acquired at *m/z* 100-500 in both ion modes. Tandem MS spectra were obtained via higher-energy collisional dissociation (HCD) with a normalized collision energy of 35.

4.3 Results and Discussion

4.3.1 Development of Chemical Derivatization of 2-AG

Various derivatization methods have been used for selective lipid detection, such as selective derivatization of phosphatidylethanolamine (PE) and lysoPE with the fluorenylmethoxylcarbonyl (Fmoc) chloride, as well as the detection of fatty acid methyl esters (FAME) with methanolic sodium methoxide, etc.[97] In these methods, native lipids are derivatized to different neutral lipids that show the improved ionization efficiencies. In our study, we develop a method that can add a charge tag to 2-AG. The charged derivative can largely increase the ion intensity of 2-AG.

The unique structural moiety in 2-AG is the diol structure, which is widely existing in carbohydrates. Previous work has illustrated the derivatization method using phenylboronic acid for carbohydrate detection and online reactive-DESI imaging.[98,99] Similarly, the phenylboronic acid was used to derivatize 2-AG because of its high reactivity with diol moiety and the potential increase in detection sensitivity and specificity.

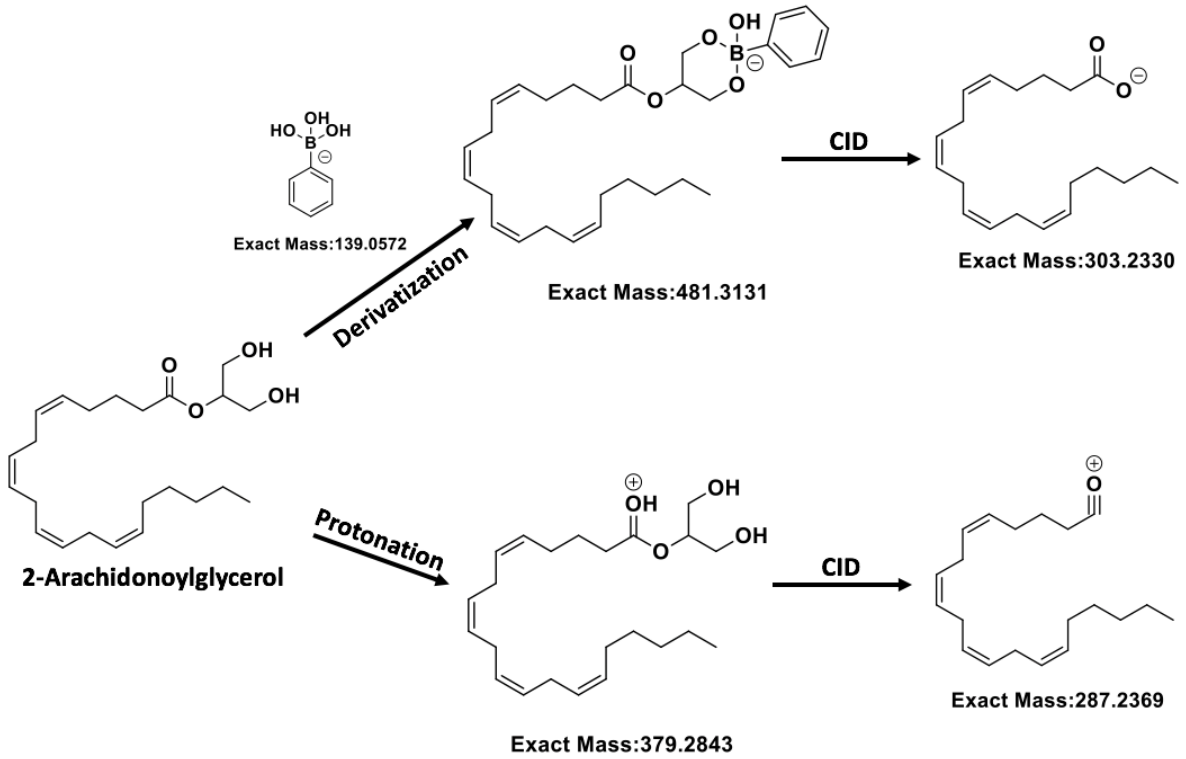

Scheme 4.1. Protonation of 2-AG and derivatization of 2-AG with phenylboronic acid as well as the formation of diagnostic fragments in HCD.

In order to demonstrate the improvement in detection specificity, derivatization method with phenylboronic acid was compared with direct protonation method (**Scheme 4.1**). Prior to nanoESI-MS analysis, the pH of 2-AG solution (100 μM, dissolved in acetonitrile/ water (80/20, v/v) containing 1 mM phenylboronic acid) was adjusted to 9 by adding ammonia solution. As shown in **Figure 4.2**, the diagnostic peak at *m/z* 303 can be readily detected with minor background peaks in the tandem mass spectrum.

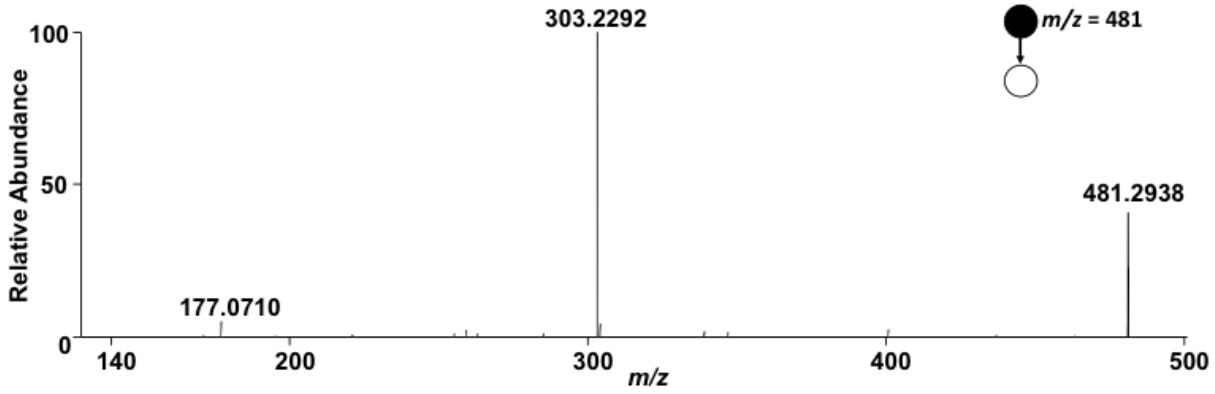

Figure 4.2. Tandem mass spectra of derivatization product at *m/z* 481, the diagnostic peak are detected at *m/z* 303.

Meanwhile, direct protonation was performed for the analysis of 2-AG solution (100 μM, dissolved in acetonitrile/ water (80/20, v/v) containing 1% formic acid) using the same set-up in chemical derivatization method. The diagnostic peak at *m/z* 287 can also be detected in the tandem mass spectrum (**Figure 4.3 a**). However, compared with the tandem mass spectrum of protonated 2-AG obtained through LC-MS (**Figure 4.3 b**), the diagnostic ion of 2-AG is not the base peak in the tandem mass spectrum, which indicated the existence of background contaminations with identical *m/z* value at 379 using direct protonation.

These results demonstrated the feasibility of chemical derivatization method with phenylboronic acid for 2-AG detection and a better detection specificity through chemical derivatization, which allows the detection of 2-AG in full MS spectrum directly.

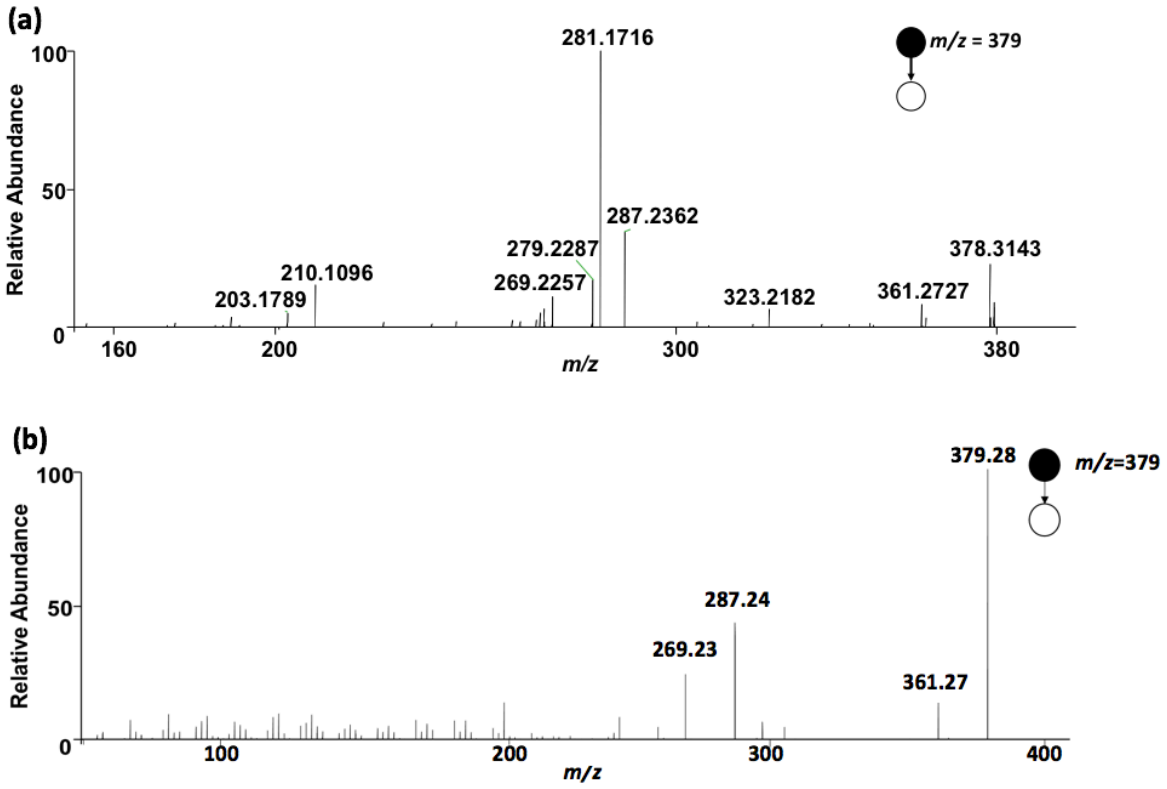

Figure 4.3. Tandem mass spectra of protonated product at *m/z* 379 detected by (a) nanoESI-MS/MS and (b) LC-MS (obtained through CID with a normalized collision energy of 30).

4.3.2 The Comparison of Detection Sensitivities in Protonation Method and Derivatization Method of 2-AG

As shown in **Figure 4.4**, the limit of detection (LOD) of the derivatization method was measured to be 1 μM, which is higher than the LOD of the protonation method (~100 nM) for 2-AG detection. However, the LOD is better than the direct analysis of 2-AG without the protonation (spectrum not shown here). Meanwhile, the diagnostic ion of the

derivatization method at *m/z* 303 was always the base peak in tandem mass spectrum within the detection limit.

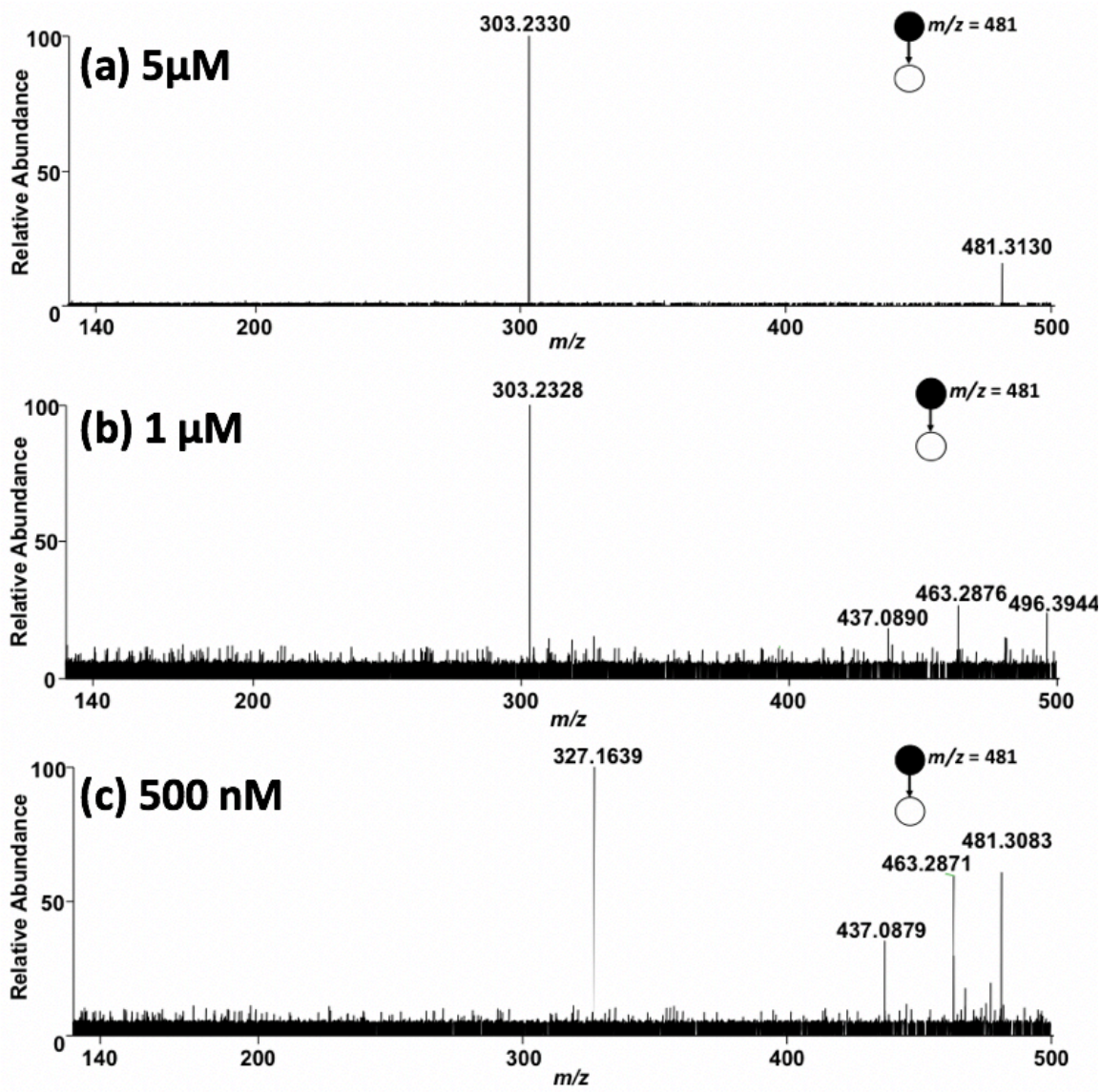

Figure 4.4. Tandem mass spectra of the derivatization product at *m/z* 481 with 2-AG concentration at (a) 5 µM, (b) 1 µM and (c) 500 nM. The LOD is estimated to be 1 µM.

4.3.3 Chemical Derivatization of 2-AG in the Lipid Extract from Mouse Brain

The direct analysis of complex sample is challenging for the protonation method because of the ion suppression from compounds with high proton affinity and the overlap with background isomeric peaks. Hyphenated techniques were usually required for pre-analysis separation to relieve the matrix effect.[93]

Chemical derivatization method of 2-AG using phenylboronic acid was performed in complex sample analysis. The lipid extract (10%, v/v) from mouse brain was dissolved in acetonitrile/ water (80/20, v/v) containing 1 mM phenylboronic acid and was analyzed through nanoESI-MS/MS. Diagnostic ion at *m/z* 303 was successfully detected in the tandem mass spectrum (**Figure 4.5**). This result shows the feasibility of the derivatization method in real sample analysis without using hyphenated techniques.

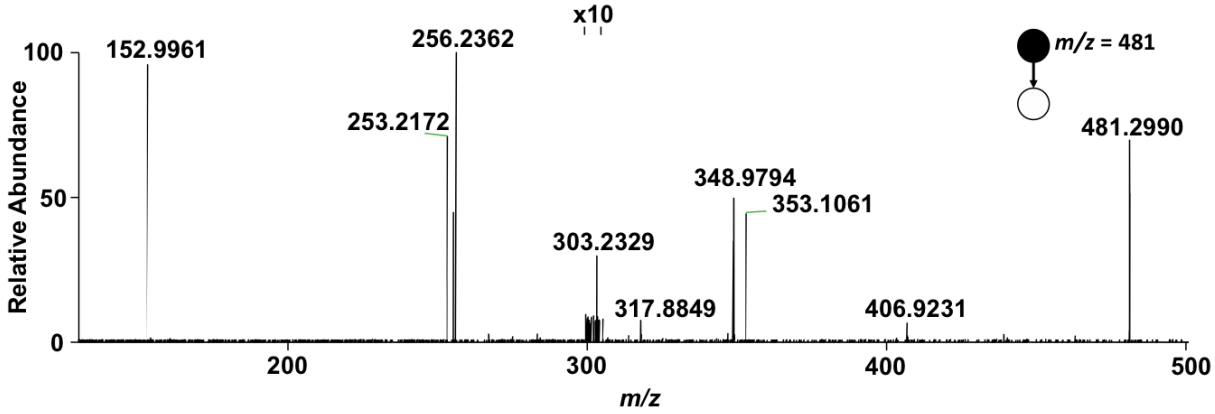

Figure 4.5. Tandem mass spectrum of derivatization product at *m/z* 481.

The experimental results demonstrate that the derivatization method using phenylboronic acid can be used for the detection of 2-AG. The detection sensitivity and specificity have been improved. The method also allows the differentiation of 2-AG in the sample from its isomeric peaks in the background, which shows the chemical derivatization method a valuable technique for low-abundance lipid species detection. The feasibility of derivatization method in real sample analysis is also demonstrated through the successful detection of 2-AG in the mouse brain lipid extract. This method provides an opportunity to analyze 2-AG in DESI imaging technique that cannot be coupled with hyphenate techniques.

5. CONCLUSIONS AND FUTURE WORK

5.1 Conclusion of the Development of an Electrochemical Mass Spectrometric Method for Double-Bond Localization in Unsaturated Lipids

The feasibility of AC-ESI combined with online electrochemical derivatization for double-bond localization in unsaturated lipids has been demonstrated in section 2. Electrospray with opposite polarities was induced by the alternating current electric field in different work cycles, respectively. Meanwhile, double-bond positional isomers were resolved with an electrochemical epoxidation in the positive half work cycle followed by the collision-induced dissociation of epoxidation products. In both ion modes, diagnostic ions for locating double-bond locations were detected in the tandem mass spectra of epoxidized lipids.

5.1.1 AC-ESI Advantages

Compared with the current derivatization approaches for double-bond positional isomer differentiation, such as ozonolysis and Paternò–Büchi reaction, AC-ESI has several advantages: i) AC-ESI makes the use of online electrochemical epoxidation, which requires no extra apparatus; ii) simultaneous detection of lipids in both ion modes in a single experiment allows a low sample consumption; iii) the controllable epoxidation which provides full MS spectra with and without epoxidation can simplify the mass

spectrum interpretation process. Moreover, AC-ESI also offers several advantages over DC-induced electrochemical epoxidation approach: i) the detection is not limited in the positive ion mode, which offers a broader range of detectable lipids; ii) simplified workflow for complex sample analysis with the detection capability of lipids in both ion modes simultaneously. Overall, AC-ESI offers the detection and double-bond positional isomer differentiation of a broad range of lipids in both ion modes simultaneously and a simplified workflow for complex sample analysis.

5.1.2 AC-ESI Limitations

AC-ESI allows the simultaneous detection of a complex mixture in both positive and negative ion modes, however, the solvent system cannot be optimal for both ion modes, which might have the signal suppression in one of the ion modes. The LOD of AC-ESI (1 μM) is also poorer than that of the previously reported DC-ESI (10 nM). However, the impaired LOD does not weaken the ability of AC-ESI to identify double-bond positional isomers in complex samples. Another consideration is the limited mechanistic study, due to the inadequate knowledge with online electrochemical epoxidation mechanism and alternating current induced electrospray mechanism, it can be hard to find the globally optimal parameters for the AC-ESI setup.

5.1.3 Identification of Lipid Isomers in the Mouse Brain Extract

The head group isomers and chain length isomers in brain extract were readily

identified through the accurate mass value, and the signature head group loss and fatty acyl chain loss peaks in CID tandem mass spectra. Nine native unsaturated lipid peaks were found to have 30 head group isomers and multiple chain length isomers.

Double-bond positional isomers in the brain extract were also analyzed using AC-ESI and a wide degree of variation in double-bond positional isomeric compositions were revealed. Five different epoxidation peaks were investigated with 15 double-bond positional isomers revealed.

For example, the study of ions at *m/z* 776 and *m/z* 802 using AC-ESI showed the presence of multiple phospholipid isomers at the identical *m/z*. For *m/z* 776, PC 16:0_18:1(Δ6), PC 16:0_18:1(Δ9) and PC 16:0_18:1(Δ11) were identified. For *m/z* 802, not only double-bond positional isomers, such as PC 18:1(Δ6)_18:1(Δ6), PC 18:1(Δ6)_18:1(Δ9), and PC 18:1(Δ9)_18:1(Δ9), were identified, the fatty acyl chain compositional isomer PC 18:0_18:2(Δ9, Δ11) was also identified in the brain extract.

5.1.4 Future Work

The application of the double-bond localization strategy using AC-ESI can proceed in many directions. AC-ESI could be used to profile a wide range of double-bond positional isomers in complex biological extracts. These lipid profile datasets could be stored in a searchable, online database. The simple set-up of AC-ESI may allow its combination with mass spectrometry imaging for double-bond positional isomer

distribution study with no need for pre-separation steps or extra apparatus. AC power supply coupled with nanoDESI-MSI can readily detect the distributions of different double-bond positional isomers, which can be used for biomarker discovery or disease diagnostics. Meanwhile, the mechanism of AC-ESI and electrochemical epoxidation will be illustrated.

5.2 Conclusion of the Discovery of Region-Specific Lipids in Mouse Brain and Biomarkers for Alcoholism using Desorption Electrospray Ionization-Mass Spectrometry Imaging

A simple approach for region identification of mouse brain in DESI-MSI images has been illustrated in section 3. Multiple brain regions including magnocellular nucleus, dorsal striatum region and brain stems were localized by specific distributions of biomarkers in MSI images. Furthermore, the datasets extracted from the identified dorsal striatum region were used for statistical analysis and a potential biomarker at *m/z* 841.83, which can be used for alcoholism sample classification and the study over pathogenesis process induced by alcoholism, was identified through multiple statistical models.

Compared with conventional adjacent tissue slice staining or post-analysis slice staining, this approach for region identification simplifies the workflow and reduces the time required for alignments. This simple region identification method is a readily approachable method for preliminary region identification in MSI study. Reliability and

accuracy of the method needs to be evaluated in the future.

A biomarker at *m/z* 841.8 (tentatively identified as triacylglycerol 51:3) was identified for alcoholism from the region-specific datasets, which demonstrates the feasibility of region-specific DESI-MSI for subtle difference detection and biomarker discovery. Some region-specific modifications, which are often overlooked in homogenized sample analysis, can be revealed using this method.

In the future, robust biomarkers may be discovered given a larger sample size, and the biochemical functions of these biomarkers in metabolic pathways can be revealed for pathological studies.

5.3 Conclusion of the Improvement of Sensitivity and Specificity in Detection of 2-Arachidonoylglycerol Using Chemical Derivatization

The chemical derivatization using phenylboronic acid was developed for 2-arachidonoylglycerol detection in section 4. Tandem mass spectrum of derivatization product at *m/z* 481 without disturbance of isomeric peaks from the background was observed through this approach. Moreover, the feasibility of the derivatization method with phenylboronic acid in real sample analysis was demonstrated through the successful detection of 2-arachidonoylglycerol in the mouse brain extract.

Further applications of chemical derivatization using phenylboronic acid for 2-AG detection are limited by the moderate detection limit of 2-AG in complex sample analysis.

In order to facilitate the chemical derivatization method in 2-AG detection, several other derivatizing agents will be tested such as 3-nitrophenylboronic acid with higher reactivity or 4-(N-methyl) pyridinium boronic acid with a permanently charge tag.[99,100] The direct detection of 2-AG in complex samples will be used in reactive-DESI-MSI to obtain the spatial distribution of 2-AG in tissues.

REFERENCES

1. Yetukuri, L., Katajamaa, M., Medina-Gomez, G., Seppänen-Laakso, T., Vidal-Puig, A., & Orešič, M. *BMC Systems Biology*, **2007**, 1(1), 12.

2. Perry, R. J., Samuel, V. T., Petersen, K. F., & Shulman, G. I. *Nature*, **2014**, 510(7503), 84-91.

3. Stegemann, C., Pechlaner, R., Willeit, P., Langley, S. R., Mangino, M., Mayr, U., & Spector, T. D. *Circulation*, **2014**, 129(18), 1821-1831.

4. Mills, G. B., & Moolenaar, W. H. *Nature Reviews Cancer*, **2003**, *3*(8), 582-591.

5. M Jeitner, T., I. Voloshyna, & A. B Reiss. *Current Medicinal Chemistry*, **2011**, 1515-1525.

6. Bagchi, Sreya, Samantha Genardi, and Chyung-Ru Wang. *Frontiers in Immunology,* **2018***,* 9, 1616.

7. Hu, Changfeng. *Free Radical Biology and Medicine,* **2016**, 475-481.

8. Musso, G., Cassader, M., Paschetta, E., & Gambino, R. *Gastroenterology*, **2018**, 155(2), 282-302.

9. Higdon, A., Diers, A. R., Oh, J. Y., Landar, A., & Darley-Usmar, V. M. *Biochemical Journal*, **2012**, 442(3), 453-464.

10. Jha, P., McDevitt, M. T., Halilbasic, E., Williams, E. G., Quiros, P. M., Gariani, K., & Coon, J. J. *Cell systems*, **2018**, 6(6), 709-721.

11. Hinterwirth, H., Stegemann, C., & Mayr, M. Circulation. *Cardiovascular Genetics*, **2014**, 7(6), 941-954.

12. Zhou, X., Mao, J., Ai, J., Deng, Y., Roth, M. R., Pound, C., ... & Bigler, S. A. *PloS One*, **2012**, 7(11).

13. Adibhatla, R. M., & Hatcher, J. F. *Antioxidants & Redox Signaling*, **2010**, 12(1), 125-169.

14. Liu, Q., & Zhang, J. *Neuroscience Bulletin*, **2014**, 30(2), 331-345.

15. Yetukuri, L., Ekroos, K., Vidal-Puig, A., & Orešič, M. *Molecular BioSystems*, **2008**, 4(2), 121-127.

16. Quehenberger, O., Armando, A. M., Brown, A. H., Milne, S. B., Myers, D. S., Merrill, A. H., ... & Sullards, C. M. *Journal of Lipid Research*, **2010**, 51(11), 3299-3305.

17. Han, X., & Gross, R. W. *Mass Spectrometry Reviews*, **2005**, 24(3), 367-412.

18. Prentki, M., Joly, E., El-Assaad, W., & Roduit, R. *Diabetes*, **2002**, 51(suppl 3), S405-S413.

19. Vickers, K. C., & Remaley, A. T. *Current Opinion in Lipidology*, **2012**, 23(2), 91-97.

20. Nagle, J. F., & Tristram-Nagle, S. *Biochimica et Biophysica Acta (BBA)-Reviews on Biomembranes*, **2000**, 1469(3), 159-195.

21. Alving, C. R. *Pharmacology & Therapeutics*, **1983**, 22(3), 407-424.

22. Chang, H. I., & Yeh, M. K. *International Journal of Nanomedicine*, **2012**, 7, 49-60.

23. Hancock, S. E., Poad, B. L., Batarseh, A., Abbott, S. K., & Mitchell, T. W. *Analytical Biochemistry*, **2017**, 524, 45-55.

24. Jesch, S. A., Liu, P., Zhao, X., Wells, M. T., & Henry, S. A. *Journal of Biological Chemistry*, **2006**, 281(33), 24070-24083.

25. Huang, M. I. N. G., Chida, K., Kamata, N., Nose, K., Kato, M., Homma, Y., & Kuroki, T. *Journal of Biological Chemistry*, **1998**, 263(34), 17975-17980.

26. Iorio, E., Mezzanzanica, D., Alberti, P., Spadaro, F., Ramoni, C., D'Ascenzo, S., & Podo, F. *Cancer Research*, **2005**, 65(20), 9369-9376.

27. Trousil, S., Lee, P., Pinato, D. J., Ellis, J. K., Dina, R., Aboagye, E. O., & Sharma, R. *Cancer Research*, **2014**, 74(23), 6867-6877.

28. Borst, J. W., Visser, N. V., Kouptsova, O., & Visser, A. J. *Biochimica et Biophysica Acta (BBA)-Molecular and Cell Biology of Lipids*, **2000**, 1487(1), 61-73.

29. Quinn, P. J., Joo, F., & Vigh, L. *Progress in Biophysics and Molecular Biology*, **1989**, 53(2), 71-103.

30. Yang, X., Sheng, W., Sun, G. Y., & Lee, J. C. M. *Neurochemistry International*, **2011**, 58(3), 321-329.

31. Micha, R., King, I. B., Lemaitre, R. N., Rimm, E. B., Sacks, F., Song, X., & Mozaffarian, D. *The American Journal of Clinical Nutrition*, **2010**, 91(4), 883-893.

32. Pfeffer, P. E., Luddy, F. E., Unruh, J., & Shoolery, J. N. *Journal of the American Oil Chemists' Society*, **1977**, 54(9), 380-386.

33. Czamara, K., Majzner, K., Pacia, M. Z., Kochan, K., Kaczor, A., & Baranska, M. *Journal of Raman Spectroscopy*, **2015**, 46(1), 4-20.

34. Sehat, N., Yurawecz, M. P., Roach, J. A., Mossoba, M. M., Kramer, J. K., & Ku, Y. *Lipids*, **1998**, 33(2), 217-221.

35. Jensen, R. G., Gordon, D. T., Heimermann, W. H., & Holman, R. T. *Lipids*, **1972**, 7(11), 738-741.

36. Hudgins, L. C., Hirsch, J., & Emken, E. A. *The American Journal of Clinical Nutrition*, **1991**, 53(2), 474-482.

37. Yang, B., Chen, H., Stanton, C., Ross, R. P., Zhang, H., Chen, Y. Q., & Chen, W. *Journal of Functional Foods*, **2015**, 15, 314-325.

38. Moss, C. W., & Lambert-Fair, M. A. *Journal of Clinical Microbiology*, **1989**, 27(7), 1467-1470.

39. Adlof, R. O. *Journal of Chromatography A*, **1996**, 741(1), 135-138.

40. Kozlowski, R. L., Campbell, J. L., Mitchell, T. W., & Blanksby, S. J. *Analytical and Bioanalytical Chemistry*, **2015**, 407(17), 5053-5064.

41. Adams, J., & Gross, M. L. *Analytical Chemistry,* **1987**, 59(11), 1576-1582.

42. K. B. Tomer, F. W. Crow, M. L. Gross, *Journal of the American Chemical Society*, **1983**, 105(16), 5487-5488.

43. Klein, D. R., Holden, D. D., & Brodbelt, J. S. *Analytical Chemistry,* **2016**, 88(1), 1044-1051.

44. Thomas, M. C., Mitchell, T. W., Harman, D. G., Deeley, J. M., Nealon, J. R., & Blanksby, S. J. *Analytical Chemistry*, **2008**, 80(1), 303-311.

45. Stinson, C. A., & Xia, Y. *Analyst*, **2016**, 141(12), 3696-3704.

46. Zhang, J. I., Tao, W. A., & Cooks, R. G. *Analytical Chemistry*, **2011**, 83(12), 4738-4744.

47. Feng, Y., Chen, B., Yu, Q., & Li, L. *Analytical Chemistry*, **2019**, 91(3), 1791-1795.

48. Tang, S., Cheng, H., & Yan, X. *Angewandte Chemie International Edition*, **2020**, 59(1), 209-214.

49. Zhao, X. E., Zhu, S., & Liu, H. *Journal of Separation Science*, **2020**, 43(9-10), 1838-1846.

50. Michell, R. H., Heath, V. L., Lemmon, M. A., & Dove, S. K. *Trends in Biochemical Sciences*, **2006**, 31(1), 52-63.

51. Sommer, U., Herscovitz, H., Welty, F. K., & Costello, C. E. *Journal of Lipid Research*, **2006**, 47(4), 804-814.

52. Basit, A., Pontis, S., Piomelli, D., & Armirotti, A. *Metabolomics*, **2016**, 12(3), 50.

53. Cajka, T., & Fiehn, O. (2014). *TrAC Trends in Analytical Chemistry*, **2014**, 61, 192-206.

54. Xiang, L., Zhu, L., Huang, Y., & Cai, Z. *Small Methods*, **2020**, 2000160.

55. Yan, Shuai, et al. *Analytical Chemistry*, **2018**, 90.11: 6362-6366.

56. Taniguchi, M., & Okazaki, T. *Biochimica et Biophysica Acta (BBA)-Molecular and Cell Biology of Lipids*, **2014**, 1841(5), 692-703.

57. Börner, K., Nygren, H., Hagenhoff, B., Malmberg, P., & Månsson, J. E. *Biochimica et Biophysica Acta (BBA)-Molecular and Cell Biology of Lipids*, **2006**, 1761(3), 335-344.

58. Eberlin, L. S., Dill, A. L., Golby, A. J., Ligon, K. L., Wiseman, J. M., Cooks, R. G., & Agar, N. Y. *Angewandte Chemie International Edition*, **2010**, 49(34), 5953-5956.

59. Milne, S., Ivanova, P., Forrester, J., & Brown, H. A. *Methods*, **2006**, 39(2), 92-103.

60. Haag, M., Schmidt, A., Sachsenheimer, T., & Brügger, B. *Metabolites*, **2012**, 2(1), 57-76.

61. Schmidt, A., Karas, M., & Dülcks, T. *Journal of the American Society for Mass Spectrometry*, **2003**, 14(5), 492-500.

62. Buchberger, A. R., DeLaney, K., Johnson, J., & Li, L. *Analytical Chemistry,* **2018**, 90(1), 240-265.

63. Chandra, S. *Applied Surface Science*, **2004**, 231-232, 467-469.

64. van Hove, E. R. A., Smith, D. F., & Heeren, R. M. *Journal of Chromatography A*, **2010**, 1217(25), 3946-3954.

65. Sparvero, L. J., Amoscato, A. A., Dixon, C. E., Long, J. B., Kochanek, P. M., Pitt, B. R., ... & Kagan, V. E. *Chemistry and Physics of Lipids*, **2012**, 165(5), 545-562.

66. Wiseman, J. M., Ifa, D. R., Song, Q., & Cooks, R. G. *Angewandte Chemie International Edition*, **2006**, 45(43), 7188-7192.

67. Pirro, V., Oliveri, P., Ferreira, C. R., González-Serrano, A. F., Machaty, Z., & Cooks, R. G. *Analytica Chimica Acta*, **2014**, 848, 51-60.

68. Valdes-Gonzalez, T., Goto-Inoue, N., Hirano, W., Ishiyama, H., Hayasaka, T., Setou, M., & Taki, T. *Journal of Neurochemistry*, **2011**, 116(5), 678-683.

69. Pasilis, S. P., Kertesz, V., Van Berkel, G. J., Schulz, M., & Schorcht, S. *Journal of Mass Spectrometry*, **2008**, 43(12), 1627-1635.

70. Cooks, R. G., Manicke, N. E., Dill, A. L., Ifa, D. R., Eberlin, L. S., Costa, A. B., ... & Ouyang, Z. *Faraday Discussions*, **2011**, 149(1), 247-267.

71. Liu, P., Lu, M., Zheng, Q., Zhang, Y., Dewald, H. D., & Chen, H. *Analyst*, **2013**, 138(19), 5519-5539.

72. Folch, J., Ascoli, I., Lees, M., Meath, J. A., & LeBaron, F. N. *Journal of Biological Chemistry*, **1951**, 191(2), 833-841.

73. Sun, C., Zhao, Y. Y., & Curtis, J. M. *Analytica Chimica Acta*, **2013**, 762, 68-75.

74. Crews, F. T., & Vetreno, R. P. *Psychopharmacology*, **2016**, 233(9), 1543-1557.

75. Bunout, D. *Nutrition*, **1999**, *15*(7-8), 583-589.

76. Zhong, W., Zhao, Y., Tang, Y., Wei, X., Shi, X., Sun, W., ... & McClain, C. J. *The American Journal of Pathology*, **2012**, 180(3), 998-1007.

77. De Almeida, I. T., Cortez-Pinto, H., Fidalgo, G., Rodrigues, D., & Camilo, M. E. *Clinical Nutrition*, **2002**, 21(3), 219-223.

78. Belin, D., & Everitt, B. J. *Neuron*, **2008**, 57(3), 432-441.

79. Tupala, E., Hall, H., Bergström, K., Mantere, T., Räsänen, P., Särkioja, T., & Tiihonen, *J. Synapse*, **2003**, 48(4), 205-211.

80. Wang, J., Carnicella, S., Phamluong, K., Jeanblanc, J., Ronesi, J. A., Chaudhri, N., & Ron, D. *Journal of Neuroscience*, **2007**, 27(13), 3593-3602.

81. Wang, J., Lanfranco, M. F., Gibb, S. L., Yowell, Q. V., Carnicella, S., & Ron, D. *Journal of Neuroscience*, **2010**, 30(30), 10187-10198.

82. Calligaris, D., Caragacianu, D., Liu, X., Norton, I., Thompson, C. J., Richardson, A. L., & Jolesz, F. A. *Proceedings of the National Academy of Sciences*, **2014**, 111(42), 15184-15189.

83. Cheng, Y., Huang, C. C., Ma, T., Wei, X., Wang, X., Lu, J., & Wang, J. *Biological Psychiatry*, **2017**, 81(11), 918-929.

84. Bokhart, M. T., Nazari, M., Garrard, K. P., & Muddiman, D. C. *Journal of The American Society for Mass Spectrometry,* **2017**, 29(1), 8-16.

85. Pang, Z., Chong, J., Li, S., & Xia, J. *Metabolites*, **2020**, 10(5), 186.

86. Puelles, L., & Rubenstein, J. L. *Trends in Neurosciences*, **2003**, 26(9), 469-476.

87. Henseler, J., Ringle, C. M., & Sinkovics, R. R. *In New Challenges to International Marketing*. **2009**.

88. Roxas, B. A., & Li, Q. *BMC Bioinformatics*, **2008**, 9(1), 187.

89. Sugiura, T., Kondo, S., Sukagawa, A., Nakane, S., Shinoda, A.,... & Waku, K. *Biochemical and Biophysical Research Communications*, **1995**, 215(1), 89-97.

90. Sugiura, T., & Waku, K. *Chemistry and Physics of Lipids*, **2000**, 108(1-2), 89-106.

91. Bisogno, T., Sepe, N., Melck, D., Maurelli, S., Petrocellis, L. D., & Marzo, V. D. *Biochemical Journal*, **1997**, 322(2), 671-677.

92. Sugiura, T., Yoshinaga, N., & Waku, K. *Neuroscience Letters*, **2001**, 297(3), 175-178.

93. Zhang, M. Y., Gao, Y., Btesh, J., Kagan, N., Kerns, E., Samad, T. A., & Chanda, P. K. *Journal of Mass Spectrometry*, **2010**, 45(2), 167-177.

94. Wang, Y., Liu, Y., Ito, Y., Hashiguchi, T., Kitajima, I., Yamakuchi, M., ... & Maruyama, I. *Analytical Biochemistry,* **2001**, 294(1), 73-82.

95. Halket, J. M., & Zaikin, V. G. *European Journal of Mass Spectrometry*, **2003**, 9(1), 1-21.

96. Wang, Y., Krull, I. S., Liu, C., & Orr, J. D. *Journal of Chromatography B*, **2003**, 793(1), 3-14.

97. Han, X., Yang, K., Cheng, H., Fikes, K. N., & Gross, R. W. *Journal of Lipid Research*, **2005**, 46(7), 1548-1560.

98. Zhu, M., Xu, X., Hou, Y., Han, J., Wang, J., Zheng, Q., & Hao, H. *Analytical Chemistry*, **2019**, 91(10), 6724-6729.

99. Springsteen, G., & Wang, B. *Tetrahedron*, **2002**, 58(26), 5291-5300.

100. Zhang, Y., & Chen, H. *International Journal of Mass Spectrometry*, **2010**, 289(2-3), 98-107.

APPENDIX

SUPPLEMENTARY MATERIALS FOR SECTION 2

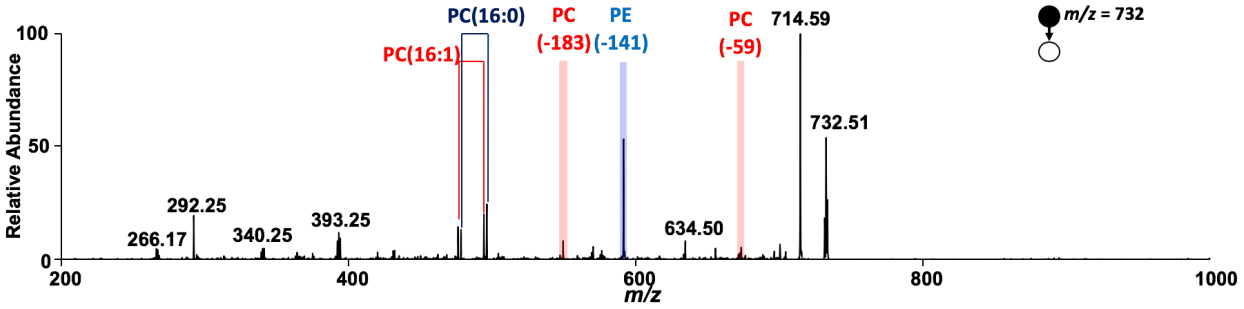

Figure A.1. Tandem Mass spectrum of native lipid at *m/z* 732. Both head group loss peaks and fatty acyl chain loss peaks are labelled.

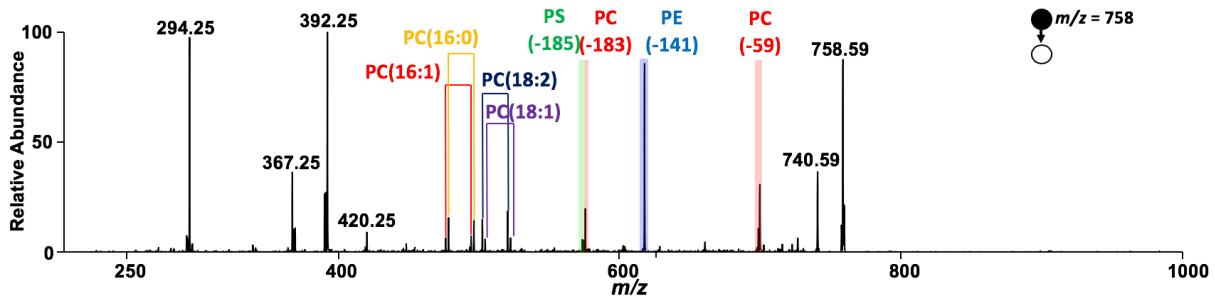

Figure A.2. Tandem Mass spectrum of native lipid at *m/z* 758. Both head group loss peaks and fatty acyl chain loss peaks are labelled.

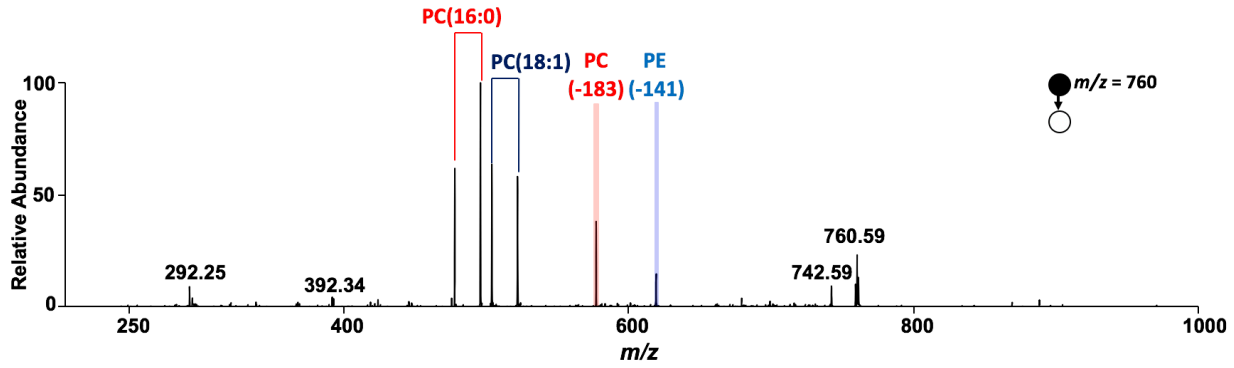

Figure A.3. Tandem Mass spectrum of native lipid at *m/z* 760. Both head group loss peaks and fatty acyl chain loss peaks are labelled.

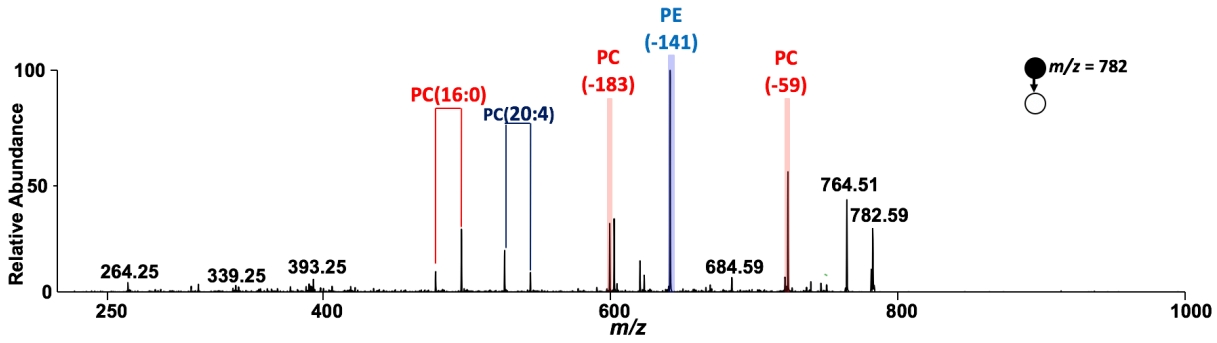

Figure A.4. Tandem Mass spectrum of native lipid at *m/z* 782. Both head group loss peaks and fatty acyl chain loss peaks are labelled.

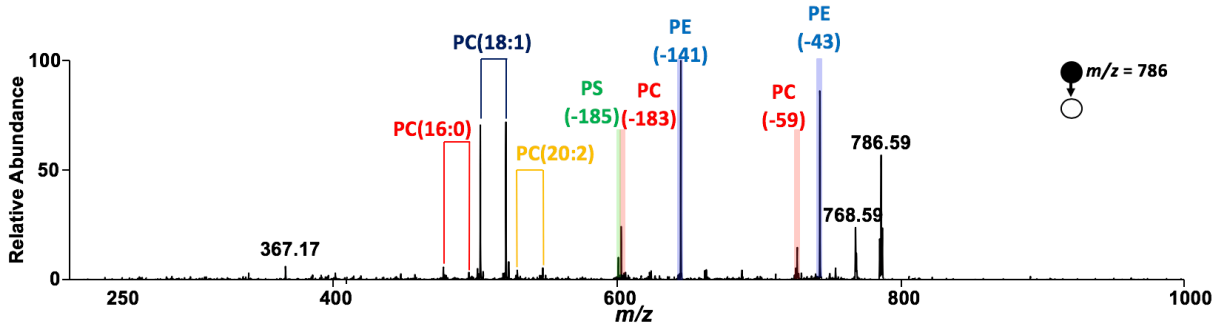

Figure A.5. Tandem Mass spectrum of native lipid at *m/z* 786. Both head group loss peaks and fatty acyl chain loss peaks are labelled.

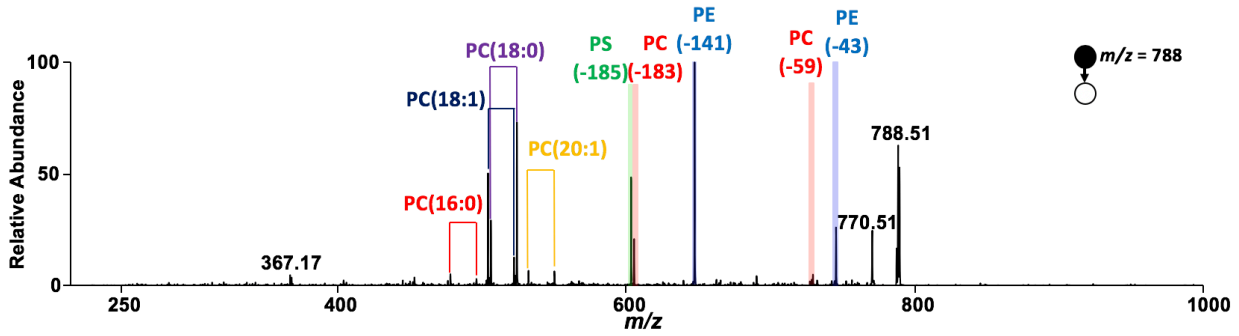

Figure A.6. Tandem Mass spectrum of native lipid at *m/z* 788. Both head group loss peaks and fatty acyl chain loss peaks are labelled.

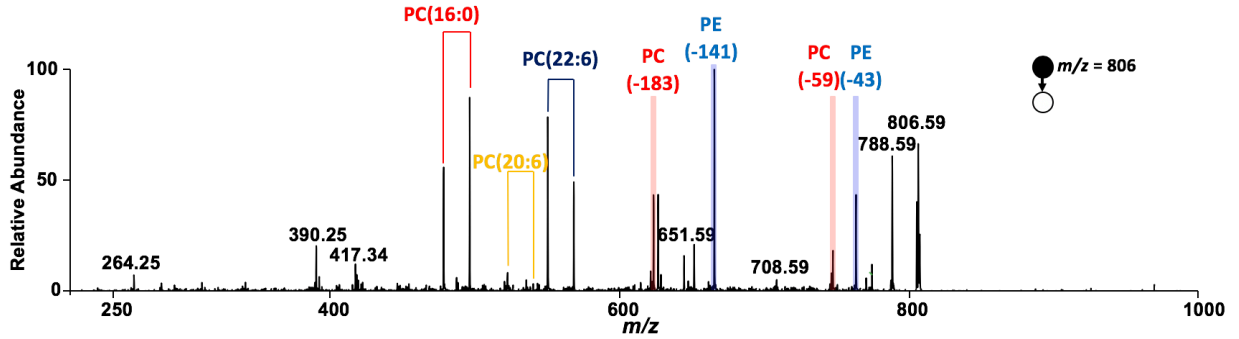

Figure A.7. Tandem Mass spectrum of native lipid at *m/z* 806. Both head group loss peaks and fatty acyl chain loss peaks are labelled.

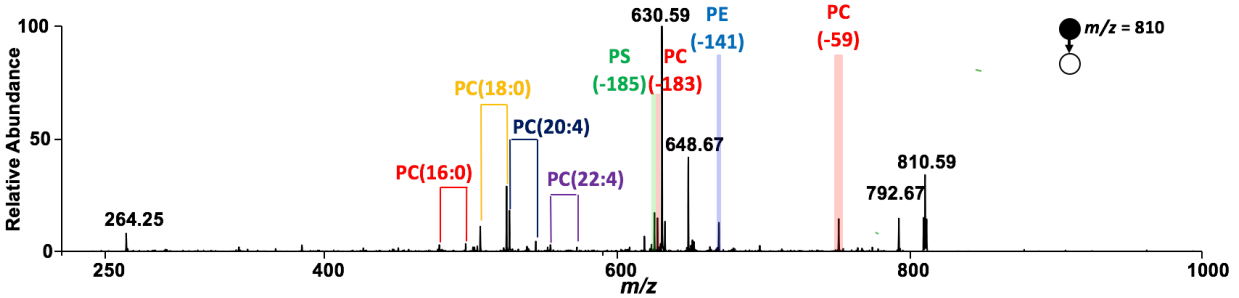

Figure A.8. Tandem Mass spectrum of native lipid at *m/z* 810. Both head group loss peaks and fatty acyl chain loss peaks are labelled.

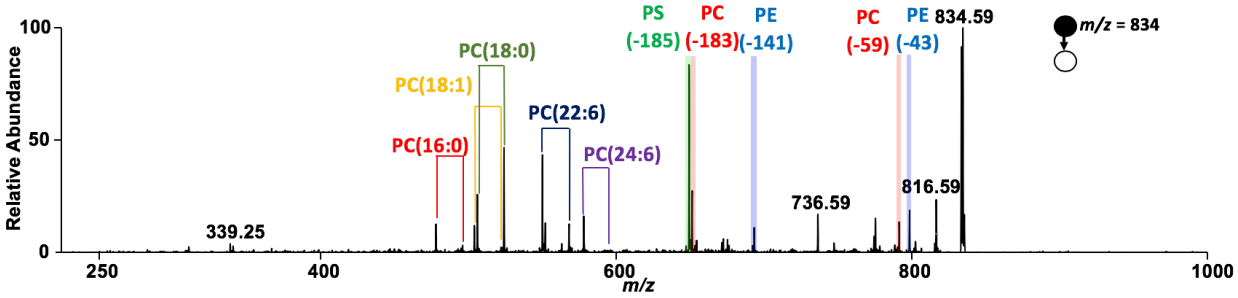

Figure A.9. Tandem Mass spectrum of native lipid at *m/z* 834. Both head group loss peaks and fatty acyl chain loss peaks are labelled.

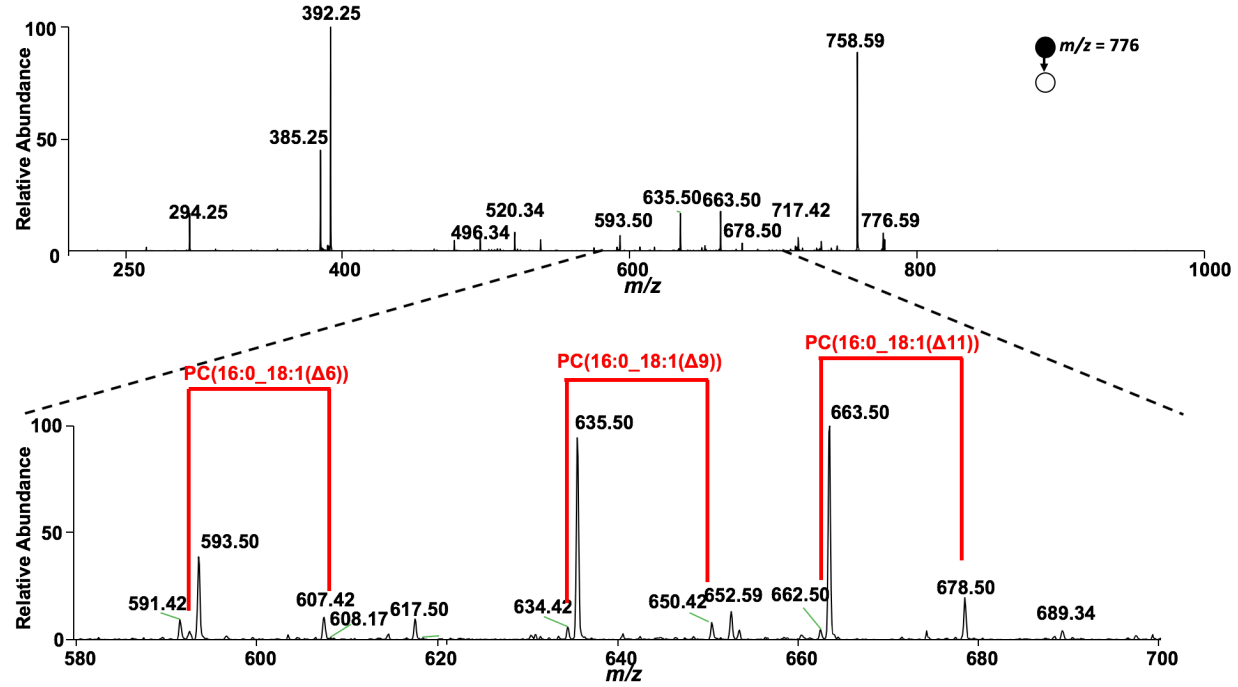

Figure A.10. Tandem Mass spectrum of epoxidized lipid at *m/z* 776. Diagnostic ions and tentative double-bond positional isomer structures are labelled.

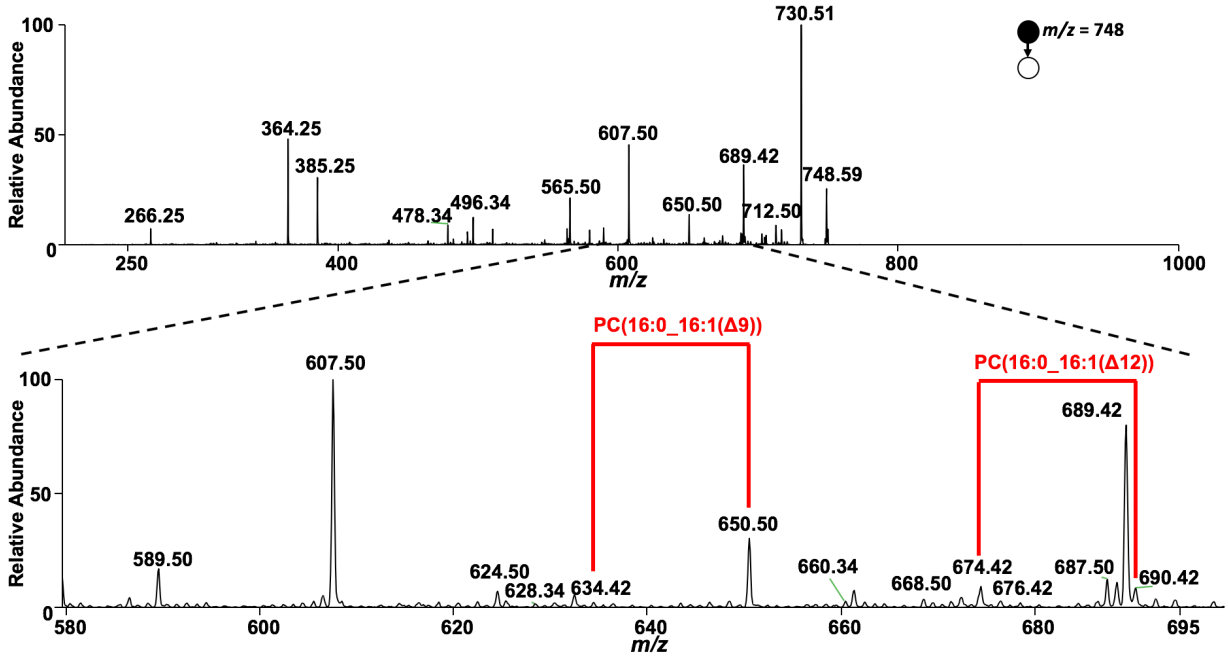

Figure A.11. Tandem Mass spectrum of epoxidized lipid at *m/z* 748. Diagnostic ions and tentative double-bond positional isomer structures are labelled.

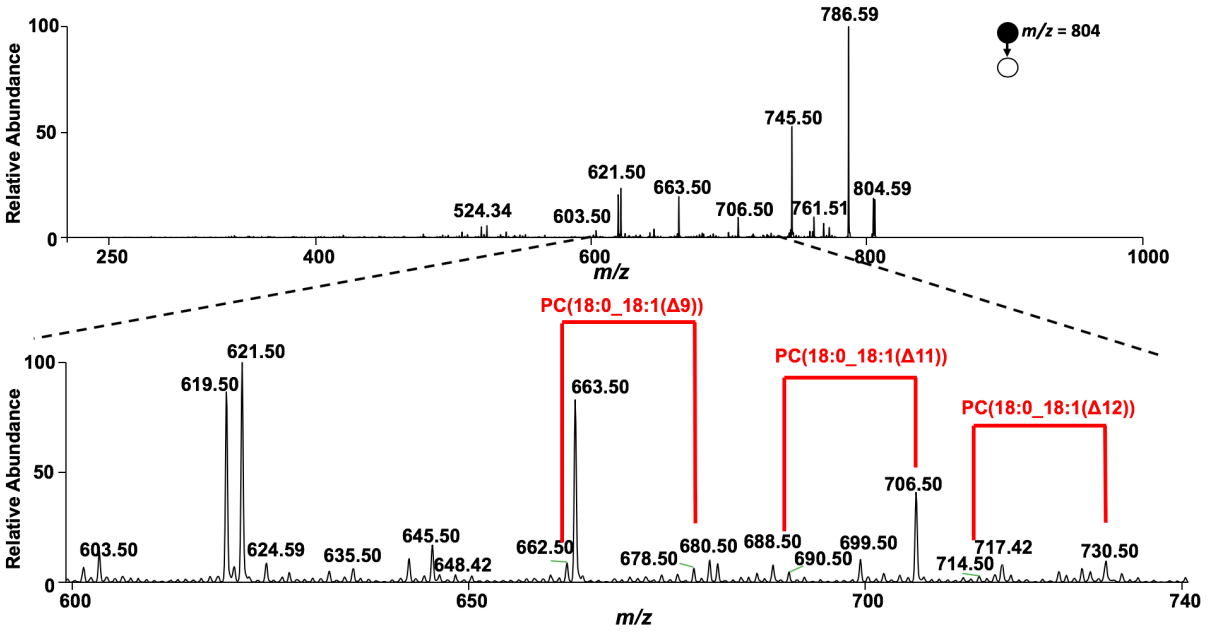

Figure A.12. Tandem Mass spectrum of epoxidized lipid at *m/z* 804. Diagnostic ions and tentative double-bond positional isomer structures are labelled.

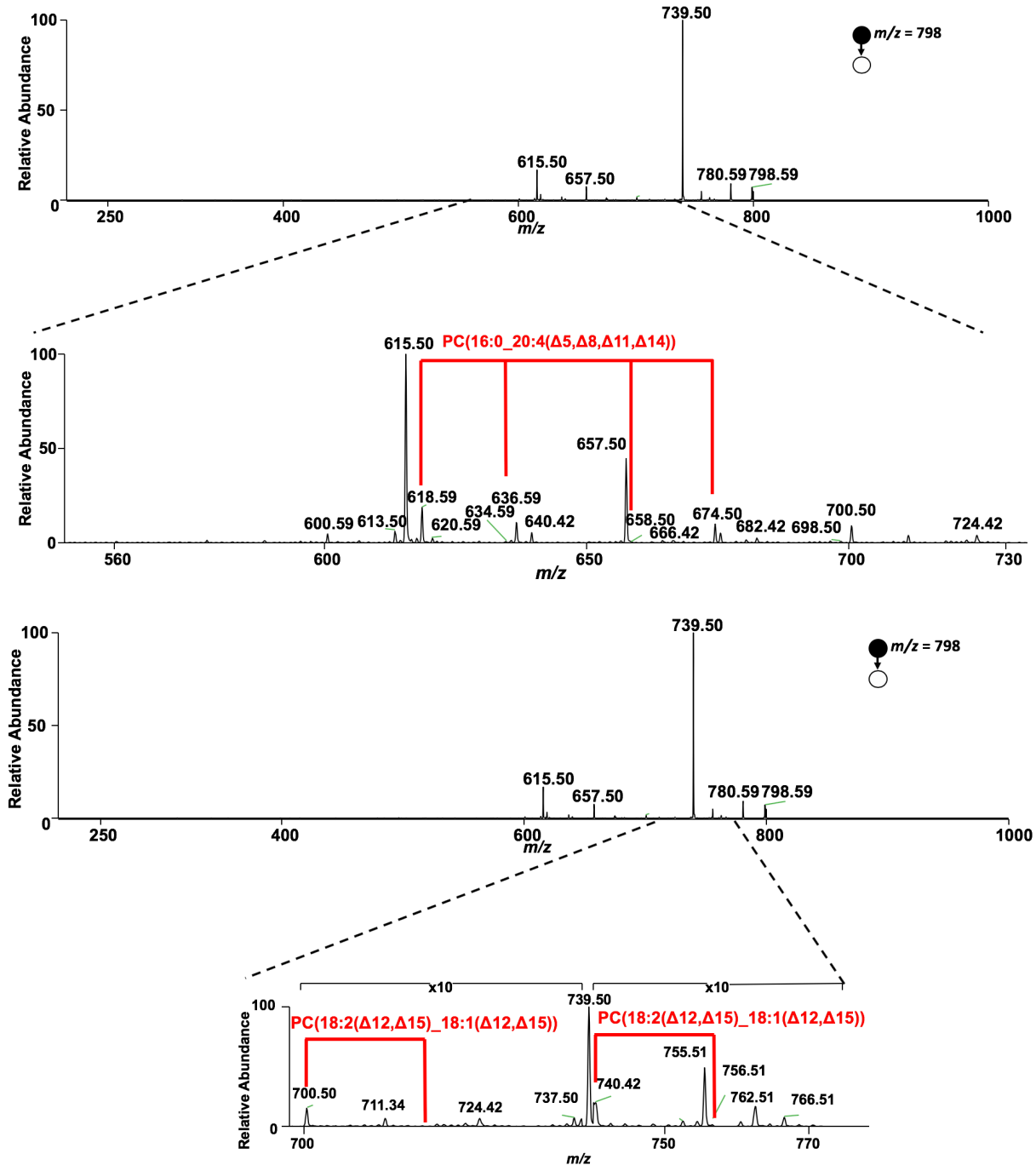

Figure A.13. Tandem Mass spectrum of epoxidized lipid at *m/z* 798. Diagnostic ions and tentative double-bond positional isomer structures are labelled.

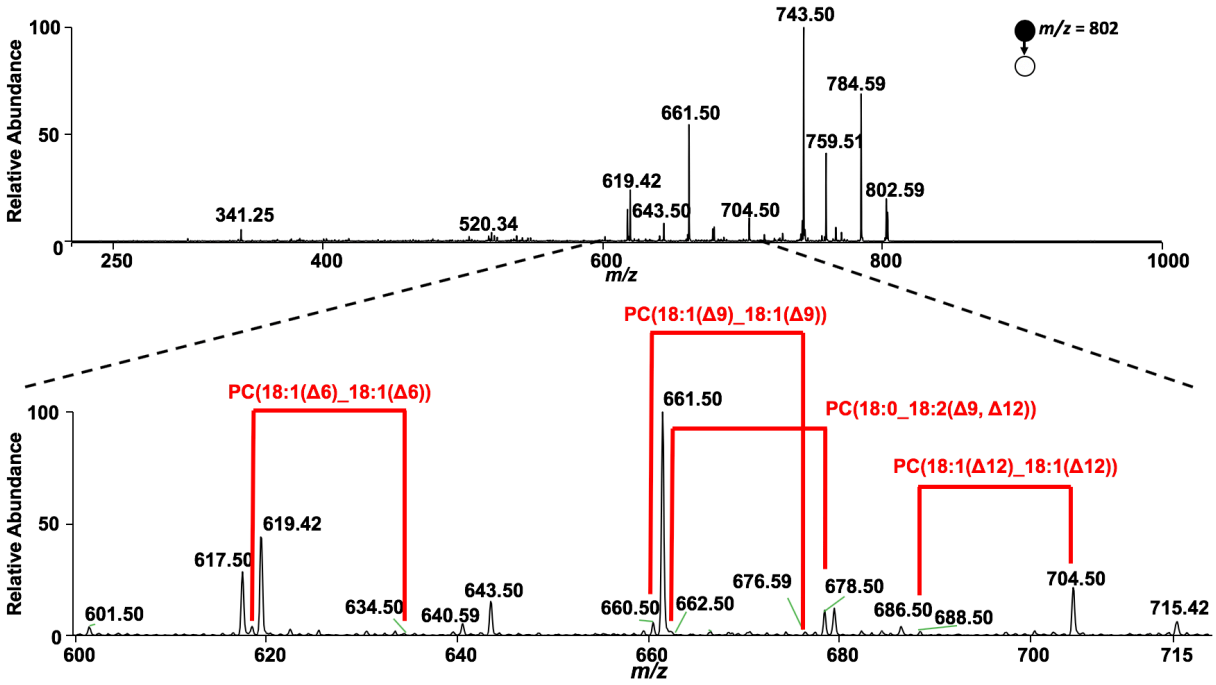

Figure A.14. Tandem Mass spectrum of epoxidized lipid at *m/z* 802. Diagnostic ions and tentative double-bond positional isomer structures are labelled.